Inhibitory CCK+ basket synapse defects in mouse models of dystroglycanopathy

Jennifer N. Jahncke[1,], Daniel S. Miller[1,], Milana Krush[1], Eric Schnell[2,3], and Kevin M. Wright[4,#]

[1] Neuroscience Graduate Program, Oregon Health & Science University, Portland, OR 97239, USA

[2] Operative Care Division, Portland VA Health Care System

[3] Anesthesiology and Perioperative Medicine, Oregon Health & Science University, Portland, OR 97239, USA

[4] Vollum Institute, Oregon Health & Science University, Portland, OR 97239, USA

[#] Correspondence to Kevin M Wright (wrighke@ohsu.edu). Vollum Institute, 3181 SW Sam Jackson Park Rd L474 Portland, OR 97239. (503)-494-6955

Keywords: dystroglycan, dystroglycanopathy, cannabinoid receptor, cholecystokinin, interneuron, synapse

Competing interests: The authors declare that they have no competing interests.

Acknowledgments
This work was funded by NIH Grants R01NS091027 (KMW), R01NS126247 (ES) CureCMD (KMW), F31NS120649 (JNJ), F31NS108522 (DSM), P30NS061800 (OHSU ALM), VA I01-BX004938 (ES), Department of Defense W81XWH-18-1-0598 (ES). The contents of this manuscript do not represent the views of the US Department of Veterans Affairs or the US government.

Author Contributions
J.N.J., D.S.M, E.S., and K.M.W. designed experiments. J.N.J, D.S.M., and M.K. performed experiments. J.N.J and D.S.M performed data analysis. J.N.J, D.S.M., and K.M.W. wrote the manuscript.

ABSTRACT

Dystroglycan (Dag1) is a transmembrane glycoprotein that links the extracellular matrix to the actin cytoskeleton. Mutations in *Dag1* or the genes required for its glycosylation result in dystroglycanopathy, a type of congenital muscular dystrophy characterized by a wide range of phenotypes including muscle weakness, brain defects, and cognitive impairment. We investigated interneuron (IN) development, synaptic function, and associated seizure susceptibility in multiple mouse models that reflect the wide phenotypic range of dystroglycanopathy neuropathology. Mice that model severe dystroglycanopathy due to forebrain deletion of *Dag1* or *POMT2*, which is required for Dystroglycan glycosylation, show significant impairment of CCK^+/CB_1R^+ IN development. CCK^+/CB_1R^+ IN axons failed to properly target the somatodendritic compartment of pyramidal neurons in the hippocampus, resulting in synaptic defects and increased seizure susceptibility. Mice lacking the intracellular domain of Dystroglycan have milder defects in $CCK^+/CB1R^+$ IN axon targeting, but exhibit dramatic changes in inhibitory synaptic function, indicating a critical postsynaptic role of this domain. In contrast, CCK^+/CB_1R^+ IN synaptic function and seizure susceptibility was normal in mice that model mild dystroglycanopathy due to partially reduced Dystroglycan glycosylation. Collectively, these data show that inhibitory synaptic defects and elevated seizure susceptibility are hallmarks of severe dystroglycanopathy, and show that Dystroglycan plays an important role in organizing functional inhibitory synapse assembly.

INTRODUCTION

The formation of neural circuits is a multistep process involving proliferation, migration, axon guidance, maturation of neuronal subtypes, and establishment of functional synaptic connections between neurons. The cell adhesion molecule Dystroglycan is widely expressed in muscle and brain. Within the forebrain, Dystroglycan is expressed in neuroepithelial cells, pyramidal neurons, astrocytes, oligodendrocytes, and vascular endothelial cells where it plays important roles in the formation of basement membranes during early brain development[1–5]. At later developmental stages, Dystroglycan is present at multiple synapses, including at photoreceptor ribbon synapses in the retina[6,7], inhibitory synapses in the cerebellum[8–10], and inhibitory synapses onto pyramidal neurons[11,12].

Dystroglycan is a central component of the dystrophin-glycoprotein complex (DGC) known primarily for its role in the etiology of neuromuscular diseases including Duchenne muscular dystrophy (DMD), limb-girdle muscular dystrophy (LGMD), and congenital muscular dystrophy (CMD). The gene encoding *Dystroglycan* (*Dag1*) yields two subunits, the extracellular alpha Dystroglycan (α-Dag1) and the transmembrane beta Dystroglycan (β-Dag1). These two subunits are non-covalently bound, allowing Dystroglycan to function as a link between extracellular ligands and cytoskeletal and signaling proteins[13–16]. Extracellular α-Dag1 interacts with multiple proteins in the nervous system through its extensive glycan chains[17]. Mutations in any of the 19 genes involved in α-Dag1 glycosylation impairs Dystroglycan function through reduced ligand binding and leads to a class of congenital muscular dystrophy termed dystroglycanopathy[18]. Patients with severe forms of dystroglycanopathy frequently

present with structural brain abnormalities and experience seizures and cognitive impairments[19–21]. Dystroglycanopathy patients with moderate severity can exhibit cognitive impairments even in the absence of identifiable brain malformations, suggesting that Dystroglycan functions at later stages of neural circuit formation such as synapse formation and/or maintenance[22,23].

The dramatic structural and anatomical phenotypes of global *Dag1* deletion in mice has often precluded analysis of Dystroglycan's synaptic functions[24–26]. Recent studies show that when *Dag1* is selectively deleted from postmitotic pyramidal neurons, neuronal migration and lamination is normal, however CCK^+/CB_1R^+ interneurons (INs) fail to populate the forebrain or form synapses in these mice[27,28]. Furthermore, conditional deletion of *Dag1* from cerebellar Purkinje neurons leads to impaired inhibitory synaptic transmission and a reduction in the number of inhibitory synapses in cerebellar cortex[9]. These studies establish a role for Dystroglycan function at a subset of inhibitory synapses in the brain, but the critical features of Dystroglycan necessary for these functions, and the relationship between inhibitory synaptogenesis and neurological phenotypes in dystroglycanopathy, remains undefined.

Here, we use multiple mouse models that recapitulate the full range of dystroglycanopathy neuropathology to address several outstanding questions related to the role of Dystroglycan at inhibitory synapses. We find that CCK^+/CB_1R^+ IN axon targeting, synapse formation, and synapse function requires both glycosylation of α-Dag1 and interactions through the intracellular domain of β-Dag1, and that defects in synaptic structure and function is associated with increased seizure susceptibility in mouse models of dystroglycanopathy.

RESULTS

Characterizing Dystroglycan localization and glycosylation in multiple models of dystroglycanopathy

While conditional deletion of *Dag1* from pyramidal neurons causes a loss of CCK^+/CB_1R^+ IN innervation in the forebrain, this has not been examined in dystroglycanopathy relevant mouse models exhibiting more widespread loss of functional Dystroglycan. We therefore generated five distinct mouse models; three to provide mechanistic insight into Dystroglycan function and two of which model mild dystroglycanopathy (schematized in **Fig. 1A**). Since complete loss of *Dag1* results in early embryonic lethality in mice, we generated forebrain-specific conditional knockouts by crossing $Emx1^{Cre}$ with *Dystroglycan* floxed mice ($Dag1^{F/F}$), to drive recombination in neuroepithelial cells in the dorsal forebrain beginning at embryonic day 10.5 (E10.5)[29]. We verified the recombination pattern of $Emx1^{Cre}$ with the mCherry reporter $Rosa26^{Lox\text{-}STOP\text{-}Lox\text{-}H2B:mCherry}$. H2B:mCherry signal was present in all excitatory neurons and astrocytes throughout the forebrain (**Supplementary Fig. 1A, B, D**) but not microglia or interneurons (**Supplementary Fig. 1C, E**).

To model loss of Dystroglycan glycosylation, $Emx1^{Cre}$ was crossed with $POMT2^{F/F}$ conditional mice to generate $POMT2^{cKOs}$. POMT2 (protein *O*-mannosyltransferase 2) is a glycosyltransferase that functions in a heterocomplex with POMT1 to add *O*-mannose at the beginning of the Dystroglycan glycan chain[30]. Without the initial *O*-mannose, no additional sugar moieties can be added to the glycan chain, resulting in near complete loss of Dystroglycan glycosylation. This is lethal

embryonically in a global *POMT2* knockout, however *Emx1*^{Cre};*POMT2*^{cKO} mice are viable and survive into adulthood[31–33].

In addition to binding extracellular ligands, Dystroglycan binds cytoskeletal proteins and signals through the intracellular tail of its β-subunit. To determine whether the intracellular domain of Dystroglycan is required for synaptic development and/or function, we examined mice in which one copy of *Dag1* was deleted, and the other copy lacks the intracellular domain of β-Dag1 (*Dag1*$^{cyto/-}$). These mice develop muscular dystrophy but show normal neuronal migration and axon guidance in regions throughout the central nervous system where Dystroglycan glycosylation is required[26,34,35].

To model mild forms of dystroglycanopathy, we examined mice expressing missense mutations in *B4GAT1 (*β-1,4-glucuronyltransferase, *B4GAT1*^{M155T}) and *FKRP* (fukutin related protein, *FKRP*^{P448L}), two genes required for Dystroglycan glycosylation. *B4GAT1*^{M155T} mice were initially identified in a forward genetic screen and develop mild muscular dystrophy and have diminished ligand binding capacity due to reduced Dystroglycan glycosylation[36]. The *FKRP*^{P448L} missense mutation models a mutation found in a patient with dystroglycanopathy[37]. In mice, the *FKRP*^{P448L} mutation leads to reduced glycosylation and mild muscular dystrophy, but no gross brain or eye malformations[18].

We first examined the pattern of Dystroglycan localization in pyramidal neurons in CA1 of hippocampus in each of the five models by immunostaining adult (P30) mice with the IIH6 antibody, which detects the terminal matriglycan repeats on the glycan chain on α-Dag1[38,39]. In wild-type (WT) mice, punctate IIH6 immunoreactivity was evident in the somatic and perisomatic compartment of CA1 pyramidal neurons (**Fig.**

1A). Immunoreactivity was also present in blood vessels, where *Dag1* is also expressed[4,40]. Neuronal immunoreactivity was undetectable in *Emx1*^{Cre}*;Dag1*^{cKOs} and *Emx1*^{Cre}*;POMT2*^{cKOs}, whereas blood vessel expression was maintained, illustrating the specificity of the conditional deletion (**Fig. 1A**). Punctate perisomatic IIH6 immunoreactivity was present in *Dag1*$^{cyto/-}$, *B4GAT1*$^{M155T/M155T}$, and *FKRP*$^{P448L/P448L}$ mice (**Fig. 1A**).

We next prepared WGA-enriched lysate from neonatal (P0) forebrain and immunoblotted for (1) IIH6, to quantify the degree of α-Dag1 glycosylation and (2) β-Dag1, to measure total Dystroglycan protein levels (**Fig. 1B**). Dag1 glycosylation was significantly reduced in *Emx1*^{Cre}*;Dag1*^{cKOs}, *Emx1*^{Cre}*;POMT2*^{cKOs}, *Dag1*$^{cyto/-}$, *B4GAT1*$^{M155T/M155T}$, and *FKRP*$^{P448L/P448L}$ mice; however, the reduction in *FKRP*$^{P448L/P448L}$ mice was less severe than the other models (**Fig. 1C**). The reduction in glycosylation observed in the *Dag1*$^{cyto/-}$ mice is surprising given that the mutation is restricted to the intracellular domain. *Dystroglycan* heterozygotes (*Dag1*$^{+/-}$) show no reduction in IIH6 levels compared to wild-types (data not shown), so the reduction in *Dag1*$^{cyto/-}$ mice can be presumed to be due to the intracellular deletion. It is possible that the intracellular domain is required for the trafficking of Dystroglycan through the endoplasmic reticulum and/or Golgi apparatus, where Dystroglycan undergoes glycosylation, however additional work is needed to verify this. As expected, β-Dag1 immunoblotting was significantly reduced in *Emx*^{Cre}*;Dag1*^{cKOs} and absent in *Dag1*$^{cyto/-}$ mice but normal in the glycosylation mutants (**Fig. 1D**). The residual β-Dag1 in *Emx1*^{Cre}*;Dag1*^{cKO} brain is likely due to *Dag1* expression in unrecombined cells, such as blood vessels, as well as unrecombined tissue that remained after the forebrain dissection.

Dystroglycan is required for cortical neuron migration in a glycosylation-dependent manner

In neocortex, *Dag1* expression in radial glia is required for proper migration of neurons, with *Dag1* conditional deletion from neuroepithelial cells or radial glia resulting in Type II lissencephaly[25,26,41,42]. This requires proper Dystroglycan glycosylation, but not its expression in neurons[36,43–45]. To compare cortical migration across our five models of dystroglycanopathy, we performed immunostaining for the upper layer marker CUX1 (layers II/III-IV) and the deep layer marker TBR1 (layers III, VI) in P30 somatosensory cortex (**Fig. 2A-B**). *Emx1*^{Cre}*;Dag1*^{cKOs} and *Emx1*^{Cre}*;POMT2*^{cKOs} showed complete cortical dyslamination with 100% penetrance, whereas the cytoplasmic (*Dag1*$^{cyto/-}$) deletion mutants appeared normal (**Fig. 2C-D**). *B4GAT1*$^{M155T/M155T}$ missense mutants showed a migration phenotype only at the cortical midline, while *FKRP*$^{P448L/P448L}$ missense mutants did not show any cortical migration phenotype (**Fig. 2 C-D, Supplementary Fig. 2A**). These results indicate that cortical migration depends on Dystroglycan glycosylation but does not require its cytoplasmic domain. Furthermore, taken with the data in **Fig. 1B-D**, they illustrate that the severity of the cortical migration phenotype scales with the degree of Dystroglycan hypoglycosylation.

Perisomatic CCK$^+$/CB$_1$R$^+$ interneuron targeting requires Dystroglycan in a non-cell autonomous manner

CCK$^+$/CB$_1$R$^+$ IN innervation is largely absent from the cortex and hippocampus when *Dag1* is deleted selectively from pyramidal neurons using *NEX*^{Cre} [27,28]. However,

the development and function of CCK^+/CB_1R^+ INs has not been examined in mouse models that more broadly lack *Dag1* throughout the central nervous system (CNS) and thus more accurately reflect the neuropathology of dystroglycanopathy. We focused our analysis on region CA1 of the hippocampus, as its overall architecture is grossly unaffected in each of our mouse models. Both *Emx1*^{Cre}*;Dag1*^{cKO} and *Emx1*^{Cre}*;POMT2*^{cKO} mice exhibited a mild granule cell migration phenotype in dentate gyrus (**Fig. 3A**, yellow arrows), however CA1-CA3 showed normal pyramidal neuron organization. In WT control mice, CCK^+/CB_1R^+ IN axon terminals were abundant throughout the hippocampus, with their highest innervation density in the CA1 pyramidal cell body layer (*stratum pyramidale*, SP) where they form characteristic basket synapses onto pyramidal neurons (**Fig. 3A-C**). In *Emx1*^{Cre}*;Dag1*^{cKO} mice, CCK^+/CB_1R^+ axons were present but failed to target the pyramidal cell layer (**Fig. 3A-C**), a marked difference from the phenotype observed in *NEX*^{Cre}*;Dag1*^{cKO} mice which lack $CCK^+/CB1R^+$ IN innervation entirely[27,28].

Emx1^{Cre}*;POMT2*^{cKO} mice fully phenocopied the aberrant *Emx1*^{Cre}*;Dag1*^{cKO} CB_1R^+ immunoreactivity pattern (**Fig. 3A-C**), demonstrating that proper CCK^+/CB_1R^+ IN basket axon targeting requires Dystroglycan glycosylation. Both the *B4GAT1* and *FKRP* mutants showed a normal distribution of CB_1R^+ axon targeting to the somatodendritic compartment of CA1 neurons, but with reduced CB_1R intensity in SP (**Fig. 3A-C**). The cytoplasmic domain of Dystroglycan also plays a role in the appropriate targeting of CB_1R immunoreactive axons, as the distribution of axons was perturbed in the *Dag1*$^{cyto/-}$ mutants, though with an intermediate phenotype in which the upper portion of SP

appeared normal while the lower portion of SP showed loss of selective CB_1R^+ axon targeting (**Fig. 3A-C**).

Due to the axonal targeting defect in the CCK^+/CB_1R^+ IN population, we next examined the parvalbumin (PV) population of interneurons in the hippocampus, as these cells also form perisomatic basket cell synapses on to CA1 pyramidal cells. The distribution of PV^+ IN axons showed normal targeting to SP in all mouse models (**Supplementary Fig. 3A-B**), indicating that the axon targeting phenotype is specific to the CCK^+/CB_1R^+ IN population. Interestingly, *Emx1*^{Cre}*;Dag1*^{cKO} mice exhibited a slight increase in PV intensity in SP, perhaps indicating that there is a degree of compensation (**Supplementary Fig. 3A-B**).

Notably, CB_1R expression was also abnormal in brain regions outside of the hippocampus. In somatosensory cortex, CB_1R immunostaining reflected the dyslamination phenotype in both the *Emx1*^{Cre}*;Dag1*^{cKO} and *Emx1*^{Cre}*;POMT2*^{cKO} mice throughout neocortex and the *B4GAT1*$^{M155T/M155T}$ mice at midline, while it appeared normal in cortex of *Dag1*$^{cyto/-}$ and *FKRP*$^{P448L/P448L}$ mice (**Supplementary Fig. 4A**). CB_1R staining was also reduced and disorganized in the basolateral amygdala (BLA) in *Emx1*^{Cre}*;Dag1*^{cKO} and *Emx1*^{Cre}*;POMT2*^{cKO} mice (**Supplementary Fig. 4B**). Interestingly, CB_1R immunostaining in the inner molecular layer (IML) of dentate gyrus appears normal in all mutants (**Fig. 3A**). In the IML, CB_1R is present in excitatory mossy cell axons targeting dentate granule cells whereas in both cortex and amygdala CB_1R expression is restricted to GABAergic interneurons[46–48]. Therefore, glycosylated Dystroglycan instructs the development of inhibitory CB_1R^+ interneuron populations in multiple brain regions.

Dystroglycan is required for CCK^+/CB_1R^+ interneuron axon targeting during early postnatal development

During early postnatal development, CCK^+/CB_1R^+ IN axons undergo a dramatic laminar rearrangement, progressing from more distal localization amongst pyramidal cell dendrites, to eventually target pyramidal neuron cell bodies in the hippocampus[28,49–51]. We examined the developmental time course of CCK^+/CB_1R^+ IN axon targeting in our *Emx1^{Cre};Dag1^{cKO}* mice beginning at P5, when the axons are first readily identifiable[52–55]. At P5 in control *Emx1^{Cre};Dag1^{Ctrl}* mice, CCK^+/CB_1R^+ axons were initially concentrated in the *stratum radiatum* (SR) of the hippocampus (**Fig. 4A-C**). Between P10 and P30, the CCK^+/CB_1R^+ axons underwent developmental reorganization, with reduced innervation of SR coinciding with a progressive increase in innervation of SP. In contrast, overall CCK^+/CB_1R^+ innervation was initially reduced in the hippocampus of mutant *Emx1^{Cre};Dag1^{cKO}* mice at P5, and these axons failed to undergo laminar reorganization as they developed (**Fig. 4A-C**). By P30, after IN synapse formation and targeting are largely complete in control mice, the density of CCK^+/CB_1R^+ axons in *Emx1^{Cre};Dag1^{cKO}* mice was uniform across all hippocampal lamina (**Fig. 4A-C**). Therefore, Dystroglycan plays a critical developmental role during the first two postnatal weeks, for the proper laminar distribution and perisomatic targeting of CCK^+/CB_1R^+ IN axons in the hippocampus.

CCK^+/CB_1R^+ IN synapse formation requires postsynaptic glycosylated Dystroglycan

Given the perturbed distribution of CCK^+/CB_1R^+ IN axons in the hippocampus, we next wanted to determine whether the remaining CCK^+/CB_1R^+ IN axons were capable of forming synapses in dystroglycanopathy models. Using VGAT as a marker of inhibitory presynaptic terminals, we saw no difference in total VGAT puncta density in SP in any of the mouse models, indicating that the total number of inhibitory synapses is normal (**Fig. 5B-D**). Immunostaining for CB_1R showed a significant decrease in CB_1R in SP of *Emx1*^{Cre}*;Dag1*^{cKO}, *Emx1*^{Cre}*;POMT2*^{cKO}, *B4GAT1*$^{M155T/M155T}$, and *FKRP*$^{P448L/P448L}$ mutants, but not *Dag1*$^{cyto/-}$ mutants (**Fig. 5E**). This suggests that the difference in CB_1R^+ axon distribution described in SP of *Dag1*$^{cyto/-}$ mutants in **Fig. 3A-C** likely reflects a change in CCK^+/CB_1R^+ IN axon targeting but not synapse formation, whereas *Emx1*^{Cre}*;Dag1*^{cKO} and all three glycosylation mutants exhibit a reduction in CCK^+/CB_1R^+ IN axon targeting and synapse number in SP. In contrast to CCK^+/CB_1R^+ INs, the PV^+ population of basket interneurons showed no change in puncta density in SP in any of the models (**Supplementary Fig. 6A-E**; analysis of VGAT, CB_1R, and PV densities in SO and SR included in **Supplementary Fig. 5A-B** and **Supplementary Fig. 7A**.)

To better approximate the extent of basket synapse formation, we quantified the co-localization between VGAT and CB_1R or PV. In SP, the percent of CB_1R puncta co-localized with VGAT was reduced in the same models that showed a reduction in CB_1R density (*Emx1*^{Cre}*;Dag1*^{cKO}, *Emx1*^{Cre}*;POMT2*^{cKO}, *B4GAT1*$^{M155T/M155T}$, and *FKRP*$^{P448L/P448L}$ mutants) but not *Dag1*$^{cyto/-}$ mutants (**Fig. 5C, F**), suggesting that CCK^+/CB_1R^+ INs require postsynaptic glycosylated Dystroglycan in order to form synapses whereas the cytoplasmic domain is required for axon targeting but not synapse formation.

Interestingly, the percent of PV co-localized with VGAT increased in the SP of *Emx1*^{Cre}*;Dag1*^{cKOs} and *Emx1*^{Cre}*;POMT2*^{cKOs} mice, with no change in any of the other models (**Supplementary Fig. 6C, E**; analysis of co-localization in SO and SR included in **Supplementary Fig. 5C**, **Supplementary Fig. 7B**). It is possible that the reduction in inhibitory CCK$^+$/CB1R$^+$ synapses prompts homeostatic compensation through an increase in PV$^+$ synapses. Alternatively, this may reflect competition between CCK$^+$/CB$_1$R$^+$ and PV$^+$ INs for physical space on the perisomatic region of pyramidal cells, with the decrease in CCK$^+$/CB$_1$R$^+$ synapses in *Emx1*^{Cre}*;Dag1*^{cKOs} and *Emx1*^{Cre}*;POMT2*^{cKOs} allowing additional PV$^+$ IN synapses to form.

CCK$^+$/CB$_1$R$^+$ interneuron basket synapse function is dependent on Dystroglycan function

Perisomatic inhibitory basket cell synapses powerfully control activity in the hippocampal circuit[56]. Previous studies in *NEX*^{Cre}*;Dag1*^{cKO} mice, in which CCK$^+$/CB$_1$R$^+$ INs are absent, demonstrated reduced inhibitory synaptic function[27]. In the current study, however, CCK$^+$/CB$_1$R$^+$ INs are present but mistargeted. Thus, we wanted to determine whether with the changes in CCK$^+$/CB$_1$R$^+$ basket synapse localization in our mouse models were associated with altered inhibitory synaptic function. CCK$^+$/CB$_1$R$^+$ IN basket cells can be selectively activated by muscarinic receptor activation, which increases the rate of spontaneous inhibitory post-synaptic currents (sIPSCs) in nearby pyramidal cells[27,57]. Thus, to assay function at CCK$^+$/CB$_1$R$^+$ IN synapses, we performed whole cell patch clamp electrophysiology from CA1 pyramidal neurons in slices from control and mutant mice. After recording 5 minutes of baseline sIPSCs, the cholinergic

receptor agonist Carbachol (CCh) was added to the bath and an additional 5 minutes of sIPSCs were recorded. While both *Emx1*^{Cre}*;Dag1*^{Ctrl} and *Emx1*^{Cre}*;Dag1*^{cKO} cells displayed a CCh-mediated increase in sIPSC frequency, this response was dramatically attenuated in *Emx1*^{Cre}*;Dag1*^{cKOs} mice compared to *Emx1*^{Cre}*;Dag1*^{Ctrl} mice (**Fig. 6A-C**). Furthermore, in *Emx1*^{Cre}*;Dag1*^{Ctrls}, 19/21 cells (90.5%) responded to CCh application (defined as a >20% increase in sIPSC frequency), whereas only 13/22 cells (59.1%) responded in *Emx1*^{Cre}*;Dag1*^{cKOs} (**Supplementary Fig. 8B**). Proper Dystroglycan glycosylation was also required for CCK^+/CB_1R^+ IN synapse function, as *Emx1*^{Cre}*;POMT2*^{cKO} mice exhibited the same phenotype as *Emx1*^{Cre}*;Dag1*^{cKOs}: a reduced response to CCh overall, and a reduced proportion of responsive cells (**Fig. 6A-C**, **Supplementary Fig. 8B**). CCh also increased the mean sIPSC amplitude in each of the controls (**Supplementary Fig. 8A**), which may reflect an increased contribution of larger-amplitude action potential-mediated perisomatic events elicited by CCh[27,57]. Consistent with the decreased function of CCK^+/CB_1R^+ IN synapses, a CCh-mediated sIPSC amplitude was also absent in each of these models (**Supplementary Fig. 8A**). Together, these data indicate that the altered perisomatic CCK^+/CB_1R^+ IN synaptic localization in CA1 is associated with a functional deficit in synaptic signaling.

Dag1$^{cyto/-}$ mutants also had dramatically attenuated sIPSC increase in CCh compared to WT controls (**Fig. 6C)**. Notably, even baseline sIPSC frequency was reduced in *Dag1*$^{cyto/-}$ mutants (2.27±1.70 Hz) compared to WT controls (4.46±2.04 Hz, $p = 0.002$), whereas baseline sIPSC frequencies appeared normal in all other mutants when compared to their respective controls. Together with the finding that these mutants contain a normal number of CCK^+/CB_1R^+ basket synapses (as measured using

immunohistochemistry; **Fig. 5A-D**), these results indicate that the cytoplasmic domain of Dystroglycan may play a critical role in mediating the assembly of functional postsynaptic signaling/receptor complexes at these synapses.

Neither of the more mildly hypoglycosylated mutants (*B4GAT1*$^{M155T/M155T}$, *FKRP*$^{P448L/P448L}$) were different from their respective littermate controls in terms of the magnitude of the CCh effect on sIPSC frequency (**Fig. 6C**), although the *B4GAT1*^{WT} mice appeared to possess a reduced effect of CCh compared to other control conditions (**Fig. 6A-C**). The *B4GAT1* line is of a mixed genetic background, which could possibly explain the difference in CCh response. This finding is of unclear significance and may have obscured potential differences. Importantly, however, the marked functional synaptic differences observed between the *Emx1*^{Cre}*;POMT2*^{cKO}, *Emx1*^{Cre}*;Dag1*^{cKO} and *Dag1*$^{cyto/-}$ mice when compared with each of their respective controls described above was not seen in either of these phenotypically milder mutants.

Together, these results suggest that Dystroglycan is required for the function of CCK^+/CB_1R^+ IN perisomatic basket synapses in a glycosylation-dependent manner, as evidenced by the *Emx1*^{Cre}*;Dag1*^{cKO} and *Emx1*^{Cre}*;POMT2*^{cKO} synaptic phenotypes, and that the intracellular domain of Dystroglycan is also required for normal CCK^+/CB_1R^+ IN basket synapse function. In contrast, *B4GAT1*$^{M155T/M155T}$ and *FKRP*$^{P448L/P448L}$ hypomorphic mutants both appear to retain sufficient Dystroglycan glycosylation to maintain normal synapse function.

Increased seizure susceptibility in models of dystroglycanopathy

Human patients with dystroglycanopathy have an increased risk of seizures and epilepsy[58–61], however the underlying cause has yet to be determined. The observed defects in inhibitory basket synapse function suggest that alterations in neuronal circuit inhibition could potentially predispose mutant mice to seizures. To test whether mouse models of dystroglycanopathy exhibit a reduced seizure threshold, we exposed mice to the volatile chemoconvulsant flurothyl and measured the latency to generalized tonic-clonic seizure (TCS)[62].

The latency to TCS was significantly faster in *Emx1*^{Cre}*;Dag1*^{cKO} mice than their littermate controls (a 40.9% reduction on average, **Fig. 7A**), with no difference in seizure latency between sexes in either group (**Supplementary Fig. 9C**). *Emx1*^{Cre}*;POMT2*^{cKOs} and *Dag1*$^{cyto/-}$ mutants also had a significantly shorter latency to TCS than littermate controls (42.9% and 33.6% reductions, respectively; **Fig. 7A**), indicating that the mechanism underlying Dystroglycan's role in seizure susceptibility requires both extracellular glycosylation and intracellular interactions. *B4GAT1*$^{M155T/M155T}$ mutants showed a small but significant reduction (16%) in seizure latency, despite exhibiting no detectable functional deficit by electrophysiology (**Fig. 6A-C**, **Fig. 7A**). Finally, *FKRP*$^{P448L/P448L}$ mutants showed no significant change in seizure susceptibility (**Fig. 7A**). These results demonstrate that disruptions in Dystroglycan function, including both its extracellular glycosylation and intracellular interactions, increase sensitivity to seizures.

DISCUSSION

Recent work identified a key role for neuronal Dystroglycan in the establishment and function of CCK^+/CB_1R^+ inhibitory synapses in the forebrain[27,28]. Deletion of *Dag1* selectively from pyramidal neurons (*NEX^{Cre};Dag1^{cKO}*) led to a near complete loss of CCK^+/CB_1R^+ INs during the first few postnatal weeks. In this study, we sought to better understand how CCK^+/CB_1R^+ IN synapse formation is affected in mouse models that more accurately reflect dystroglycanopathy, in which Dystroglycan function is more broadly affected throughout the CNS (**Figs. 1**, **2**). Using a model that deletes *Dag1* throughout the developing forebrain (*Emx1^{Cre};Dag1^{cKO}*) we found that CCK^+/CB_1R^+ INs were present, but the laminar organization of their axon terminals and their ability to form functional basket synapses onto pyramidal neuron cell bodies in the hippocampus was impaired (**Figs. 3-6**). The inability of CCK^+/CB_1R^+axon terminals to concentrate in the CA1-3 cell body layer began to manifest during the first postnatal week, when dynamic changes in laminar innervation by CCK^+/CB_1R^+ axons normally occur (**Fig. 4**). Furthermore, these mice were found to exhibit a reduced seizure threshold compared to controls, showing for the first time that mouse models of dystroglycanopathy are vulnerable to seizures (**Fig. 7**). Because the *Emx1^{Cre}* conditional deletion of *Dag1* or *POMT2* leads to widespread loss of functional Dystroglycan in the forebrain in contrast with the previously studied *NEX^{Cre}* conditional deletion, which targets pyramidal neurons, these models more accurately model dystroglycanopathy.

We found that CCK^+/CB_1R^+ IN synapse formation and function are dependent on proper Dystroglycan glycosylation and appear to correlate with the degree of hypoglycosylation in different mutants. Complete reduction of glycosylation in

Emx1^{Cre}*;POMT2*^{cKO} mutants caused the same phenotypes seen in Dystroglycan conditional knockouts (*Emx1*^{Cre}*;Dag1*^{cKO}) (**Figs. 1-3, 5-6**). A milder reduction in glycosylation (*B4GAT1*$^{M155T/M155T}$) resulted in a cortical migration phenotype that was restricted to midline (**Supplementary Fig. 4**) and a small reduction in CCK^+/CB_1R^+ axon terminals and synaptic puncta density in CA1 which did not appear to affect synapse function (**Figs. 3, 5-6**). The mildest reduction in glycosylation amongst our models was observed in *FKRP*$^{P448L/P448L}$ mutants, which exhibited normal cortical migration but the same mild defect in CCK^+/CB_1R^+ IN axon targeting and synaptic puncta density observed in *B4GAT1*$^{M155T/M155T}$ mutants (**Figs. 3, 5-6**). Together, these three glycosylation mutants illustrate the degree of hypoglycosylation required for neurodevelopmental processes and show that defects in synaptic function only arise in the context of severely reduced glycosylation; the residual Dystroglycan function present in *B4GAT1*$^{M155T/M155T}$ and *FKRP*$^{P448L/P448L}$ mutants is sufficient for most aspects of brain development. Finally, using *Dag1*$^{cyto/-}$ mutants that lack the intracellular domain of Dystroglycan, we found that the intracellular domain plays a role in some, but not all, neurodevelopmental processes. The intracellular domain is not required for neuronal migration in neocortex or synapse formation in CA1 (**Figs. 2 and 5**) but is required for the proper targeting of CCK^+/CB_1R^+ IN axons in CA1-3 (**Fig. 3**) and for subsequent CCK^+/CB_1R^+ IN basket synapse function (**Fig. 6**).

Dystroglycan is an essential transsynaptic organizing molecule for CCK^+/CB_1R^+ basket synapses

Synaptogenesis requires multiple distinct steps: (1) synaptic partner recognition, (2) recruitment and assembly of core pre- and post-synaptic machinery, (3) differentiation and maturation of synaptic identity, and (4) synaptic maintenance[63]. Based on data from this study (**Fig. 4**) and previous work from our group and others, mice lacking *Dystroglycan* exhibit defects in CCK^+/CB_1R^+ IN development at the earliest time point they can be reliably identified (P0-P5), before the peak phase of inhibitory synapse formation (P9), suggesting that Dystroglycan functions at the earliest stages of synaptogenesis such as synaptic partner recognition[64]. Determining the precise onset of synapse targeting and formation for most IN subtypes, including CCK^+/CB_1R^+INs, is limited by a lack of genetic tools for visualizing and manipulating IN subtypes during developmental stages.

The impairment in CCK^+/CB_1R^+ IN development throughout the forebrain suggests a trans-synaptic role for Dystroglycan **(Fig. 3, Supplementary Fig. 4**). The identity of the trans-synaptic binding partner between Dystroglycan-expressing cells and CCK^+/CB_1R^+ INs remains unknown. Our data in *Emx1*^{Cre}*;POMT2*^{cKO} mice point to a critical role for the glycan chains on Dystroglycan mediating this binding. All proteins that bind to the glycan chains on Dystroglycan do so through at least one Laminin G (LG) domain. There are over 25 LG-domain containing extracellular or transmembrane proteins expressed in the hippocampus. Neurexins, a family of highly alternatively spliced synaptic cell-adhesion molecules (*NRXN1-3*) which each contain multiple LG domains, bind Dystroglycan in a glycosylation-dependent manner[65–68]. The specific splice isoforms of *Nrxns* that bind Dystroglycan are expressed by CCK^+/CB_1R^+ INs[66,69]. *Neurexin-3* conditional knockout (targeting all *Nrxn3* isoforms) and CRISPR-mediated

Dag1 knockout both result in similar synaptic deficits in olfactory bulb and prefrontal cortex[70]. While a Dystroglycan knock-in mouse with reduced glycosylation that impairs Neurexin binding (*Dag1*^{T190M}) shows normal CCK^+/CB_1R^+ synapse formation by immunohistochemistry, the functionality of these synapses was not assessed by electrophysiology[27]. Similar to *B4GAT1*$^{M155T/M155T}$ and *FKRP*$^{P448L/P448L}$ mutants, the *Dag1*^{T190M} mutation does not fully eliminate Dystroglycan glycosylation, and therefore does not rule out the possibility that Neurexins play a role at CCK^+/CB_1R^+ synapses. It is also possible that a yet undescribed Dystroglycan interacting protein is required for initial synapse recognition, and Nrxn-Dag1 interactions are required for subsequent synapse maturation and maintenance only. Indeed, the majority of studies indicate that Neurexins are not required for the initial formation of synapses, but rather regulate the maturation and structural maintenance of synapses after they have formed[70–74]. Interestingly, while Dystroglycan localizes to both PV^+ and CCK^+/CB_1R^+ inhibitory basket synapses in CA1, only the CCK^+/CB_1R^+ IN population was affected in the dystroglycanopathy models[27]. Presumably, PV^+ INs have a distinct developmental program independent of Dystroglycan and likely require a different postsynaptic recognition partner.

A role for the Dystrophin-Glycoprotein Complex (DGC) in CCK^+/CB_1R^+ interneuron development

In brain and muscle tissue, Dystroglycan forms a complex with Dystrophin and several other proteins, collectively known as the Dystrophin Glycoprotein Complex (DGC). Like Dystroglycan, Dystrophin is also expressed throughout the forebrain and is

associated with inhibitory synapses in multiple brain regions[75]. Patients with mutations in *Dystrophin* develop Duchenne Muscular Dystrophy (DMD), and frequently exhibit cognitive impairments in the absence of brain malformations, suggesting a general role for the DGC in synapse development and function[76–78]. A mouse model of DMD lacking all neuronal Dystrophin isoforms (*mdx*) exhibits defects in CCK^+/CB_1R^+ IN synapse development and abnormal innervation in the hippocampus, resembling the innervation pattern we observed in $Emx1^{Cre};Dag1^{cKO}$ and $Emx1^{Cre};POMT2^{cKO}$ mice in this study[79]. Since Dystroglycan interacts with Dystrophin through its intracellular domain, we expected to observe similar phenotypes in mice lacking the intracellular domain of Dystroglycan ($Dag1^{cyto/-}$). However, $Dag1^{cyto/-}$ showed a milder axon targeting defect than $Emx1^{Cre};Dag1^{cKO}$ or *mdx* mice. In addition, IIH6 puncta were normally localized to the somatodendritic compartment in $Dag1^{cyto/-}$ mutants, suggesting that Dystroglycan does not require interactions with Dystrophin for is localization to somatodendritic synapses. However, Dystroglycan's synaptic localization has not been examined in the *mdx* mutants. Clearly, additional work is required to better understand the relationship between Dystroglycan and Dystrophin at synapses in the brain.

While the density of CCK^+/CB_1R^+ IN synaptic puncta was normal in $Dag1^{cyto/-}$ mice, synaptic function was impaired to the same level as $Emx1^{Cre};Dag^{cKO}$ and $Emx1^{Cre};POMT2^{cKO}$ mice, and seizure latency was reduced. Given that $Dag1^{cyto/-}$ and $B4GAT1^{M155T/M155T}$ mutants show a similar reduction in Dystroglycan glycosylation (**Fig. 1B-C**), our observation that the functional synaptic phenotype is restricted to the $Dag1^{cyto/-}$ mutant reinforces the notion that the intracellular domain of Dystroglycan plays an active role in organizing essential postsynaptic signaling elements. One

possibility is that the intracellular domain of Dystroglycan is required to recruit additional postsynaptic scaffolding elements and receptors necessary for CCK^+/CB_1R^+ basket synapse function[80]. Importantly, *Dag1*$^{cyto/-}$ mice did not show a cortical migration phenotype (**Fig. 2A-D**), indicating that the functional synaptic deficits and reduced seizure latency occurred independent of cortical malformation.

Altered inhibitory synapse development and function may contribute to neurological symptoms in dystroglycanopathy

In addition to muscular atrophy and hypotonia, dystroglycanopathy patients often present with central nervous system symptoms. Patients with the most severe forms of dystroglycanopathy (FCMD, muscle-eye-brain disease, and Walker-Warburg Syndrome) exhibit structural changes including hypoplasia of the retina, brainstem and spinal cord, cerebellar cysts, hydrocephalus, type II lissencephaly, and microcephaly, associated with seizures and cognitive disability[81,82]. Patients with milder forms of dystroglycanopathy may show cognitive disability and/or seizures without gross brain malformations, suggesting that there may be synaptic deficits independent of early neurodevelopmental processes (e.g. neuronal migration, axon guidance)[58,82]. Mutations in any of the genes involved in the glycosylation of Dystroglycan can result in dystroglycanopathy with seizures, but the incidence and severity of seizures is higher in patients with brain malformations[58,82,83].

Mice have been used to model dystroglycanopathy for decades, however to our knowledge the present study is the first to investigate seizure susceptibility in mouse models of dystroglycanopathy. It is probable that the CCK^+/CB_1R^+ interneuron axon

targeting and synapse phenotypes in the mouse models described in the present study contribute to their seizure susceptibility and open the possibility that defective inhibitory synaptic signaling mechanisms may underlie seizures in dystroglycanopathy patients. Although severe neuronal migration phenotypes In *Emx1*^{Cre}*;Dag1*^{cKO} and *Emx1*^{Cre}*;POMT2*^{cKO} mice may contribute to seizure activity, our observation that *Dag1*$^{cyto/-}$ mutants showed both abnormal CCK^+/CB_1R^+synaptic function and reduced seizure latency, with intact cortical migration, indicates that the seizure phenotype is likely associated with synaptic defects.

While our *B4GAT1*$^{M155T/M155T}$ mutants showed only a slightly reduced seizure latency, the mutants experienced more severe seizures than the other mouse models, resulting in death in 50% of cases (4/8 mutants compared to 0/6 fatalities among littermate controls) (**Supplementary Fig. 9A**). Flurothyl-induced seizures are typically generalized forebrain seizures; however in seizure-prone mouse models or in mice exposed to higher concentrations of flurothyl, mice can experience a suppression of brainstem oscillations followed by sudden death[84,85]. The *B4GAT1*$^{M155T/M155T}$ mutation was originally identified based on a hindbrain axon guidance phenotype, suggesting they may have currently unknown defects in brainstem development or circuitry that could render them more susceptible to fatal brainstem seizures[36]. Because the *Dag1* and *POMT2* mutants are forebrain-specific conditional knockouts, (**Supplementary Fig. 1A**), we would not anticipate abnormal axon guidance in the brainstem or hindbrain of these mutants. Further research on the nature and progression of seizures observed in mouse models may have a profound impact on our understanding of dystroglycanopathy and potential therapeutic interventions.

Potential therapeutics for the restoration of synapse function in patients with dystroglycanopathy

Most patients with dystroglycanopathy present with mutations in one of the 19 genes required for the glycosylation of Dystroglycan, resulting in hypoglycosylated Dystroglycan. We have demonstrated that a mild reduction in the glycosylation of Dystroglycan, as seen in *FKRP*$^{P448L/P448L}$ and *B4GAT1*$^{M155T/M155T}$ mutants, does not significantly disrupt synapse function. This suggests that glycosylation may not need to be restored to wild-type levels in order to achieve normal synapse function. Gene replacement therapy may be well suited to treat certain forms of dystroglycanopathy by rescuing glycosylation. AAV-mediated delivery of fully functional glycosyltransferases has been shown to significantly improve muscle pathology and function in dystrophic mice, however synaptic phenotypes have not been examined[86]. Supplementation with (CDP)-ribitol, which is synthesized by *CRPPA* (previously known as *ISPD*), can restore functional Dystroglycan glycosylation and improve muscle function in mouse models with hypomorphic mutations in *CRPPA* or *FKRP*[87]. In mice lacking functional *CRPPA* or *FKRP* in skeletal muscle, (CDP)-ribitol can further enhance the therapeutic impact of gene restoration[88]. However, whether (CDP)-ribitol treatment can improve Dystroglycan function in other models of dystroglycanopathy, or is capable of restoring Dystroglycan glycosylation and synaptic function in the nervous system, remains untested.

CONCLUSION

We demonstrate that Dystroglycan is critical for the postnatal development of CCK^+/CB_1R^+ interneuron axon targeting and synapse formation/function in the hippocampus of severe mouse models of dystroglycanopathy. Extracellular glycosylation of Dystroglycan and intracellular interactions involving the cytoplasmic domain are both essential for Dystroglycan's synaptic organizing role. Mice with a partial reduction in glycosylation have relatively normal CCK^+/CB_1R^+ interneuron axon targeting and synapse function, suggesting that even a partial restoration of glycosylation may have some therapeutic benefit. These findings suggest that CCK^+/CB_1R^+ interneuron axon targeting defects may contribute to cognitive impairments and seizure susceptibility in dystroglycanopathy.

MATERIALS AND METHODS

Animal husbandry

All animals were housed and cared for by the Department of Comparative Medicine (DCM) at Oregon Health and Science University (OHSU), an AAALAC-accredited institution. Animal procedures were approved by OHSU Institutional Animal Care and Use Committee (Protocol # IS00000539), adhered to the NIH *Guide for the care and use of laboratory animals*, and provided with 24-hour veterinary care. Animal facilities are regulated for temperature and humidity and maintained on a 12-hour light-dark cycle and were provided food and water *ad libitum*. Animals older than postnatal day 6 (P6) were euthanized by administration of CO_2, animals <P6 were euthanized by rapid decapitation,

Mouse strains and genotyping

The day of birth was designated postnatal day 0 (P0). Ages of mice used for each analysis are indicated in the figure and figure legends. Mouse strains used in this study have been previously described and were obtained from Jackson Labs, unless otherwise indicated (**Table 1**)[35,36,43,44,89–91]. Breeding schemas are as described in **Table 2**. Where possible, mice were maintained on a C57BL/6 background. *Dag1*$^{cyto/-}$ mice occurred at a frequency lower than Mendelian, suggesting that a proportion of progeny die embryonically. To increase viability of pups, the *Dag1*^{cyto} line was outcrossed to a CD-1 background for one generation. The *B4GAT1* line has a mixed genetic background: it was founded on a C3H/He background and then crossed on to C57BL/6 for future generations. Genomic DNA extracted from toe or tail samples (Quanta BioSciences) was used to genotype animals. Primers for genotyping can be found on the JAX webpage or originating article. For each mouse strain, littermate controls were used for comparison with mutant mice.

Table 1. Mouse strains

Common name	Strain name	Reference	Stock #
Dag1^{Flox}	*B6.129(Cg)-Dag1*$^{tm2.1Kcam}$*/J*	Cohn et al., 2002[89]	009652
Dag1^{cyto}	N/A	Satz et al., 2009[35]	N/A
POMT2^{Flox}	*POMT2tm1.1Hhu/J*	Hu et al., 2011[43]	017880
B4GAT1^{M155T}	*B6(C3)-B4GAT1*^{m1Ddg}*/J*	Wright et al., 2012[36]	022018
Fkrp^{P448L}	C57BL/6NJ-Fkrp^{em1Lgmd}/J	Chan et al., 2010[44]	034659
R26$^{LSL-H2B-mCherry}$	*B6.Gt(ROSA)26Sor*$^{tm1.1Ksvo}$	Peron, et al., 2015[90]	023139
Emx1^{Cre}	*B6.129S2-Emx1*$^{tm1(cre)Krj}$*/J*	Gorski et al., 2002[91]	005628

Table 2. Breeding schemes

Breeding Scheme	Control Genotype	Mutant Genotype
Emx1$^{Cre/+}$;Dag1$^{+/-}$ x Dag1$^{Flox/Flox}$	*Emx1$^{Cre/+}$;Dag1$^{Flox/+}$*	*Emx1$^{Cre/+}$;Dag1$^{Flox/-}$*
Emx1$^{Cre/+}$;POMT2$^{Flox/+}$ x POMT2$^{Flox/Flox}$	*Emx1$^{Cre/+}$;POMT2$^{Flox/+}$*	*Emx1$^{Cre/+}$;POMT2$^{Flox/Flox}$*
Dag1$^{cyto/+}$ x Dag1$^{+/-}$	*WT*	*Dag1$^{cyto/-}$*
B4GAT1$^{M155T/+}$ x B4GAT1$^{M155T/+}$	*WT*	*B4GAT1$^{M155T/M155T}$*
FKRP$^{P448L/+}$ x FKRP$^{P448L/+}$	*WT*	*FKRP$^{P448L/P448L}$*

Perfusions and tissue preparation

Brains from mice younger than P15 were dissected and drop fixed in 5 mLs of 4% paraformaldehyde (PFA) in phosphate buffered saline (PBS) overnight for 18-24 hours at 4°C. Mice P15 and older were deeply anesthetized using CO2 and transcardially perfused with ice cold 0.1M PBS for two minutes to clear blood from the brain, followed by 15 mLs of ice cold 4% PFA in PBS. After perfusion, brains were dissected and post-fixed in 4% PFA for 30 minutes at room temperature. Brains were rinsed with PBS, embedded in 4% low-melt agarose (Fisher cat. no. 16520100), and sectioned at 50µm using a vibratome (VT1200S, Leica Microsystems Inc., Buffalo Grove, IL) into 24-well plates containing 1 ml of 0.1M PBS with Sodium Azide.

Immunohistochemistry

Single and multiple immunofluorescence detection of antigens was performed as follows: free-floating vibratome sections (50µm) were briefly rinsed with PBS, then blocked for 1 hour in PBS containing 0.2% Triton-X (PBST) plus 10% normal goat or donkey serum. Sections were incubated with primary antibodies (**Table 3**) diluted in blocking solution at 4°C for 48-72 hours. For staining of Dystroglycan synaptic puncta, an antigen retrieval step was performed prior to incubation in primary antibody. Briefly, sections were incubated in sodium citrate solution for 15 min at 95 degrees in a water

bath. Following incubation in primary antibody, sections were rinsed with PBS then washed with PBST three times for 20 min each. Sections were then incubated with a cocktail of secondary antibodies (1:500, Alexa Fluor 488, 546, 647) in blocking solution overnight at room temperature. Sections were washed with PBS three times for 20 min each and counterstained with Hoechst 33342 (1:10,000, Life Technologies, Cat# H3570) for 20 min to visualize nuclei. Finally, sections were mounted on slides using Fluoromount-G (SouthernBiotech) and sealed using nail polish.

Table 3. Primary antibodies used for immunohistochemistry

Target	Host	Dilution	Source	Catalog #	RRID
α-Dystroglycan (IIH6C4)	Mouse	1:250	Millipore	05-593	AB_309828
CB1R	Guinea pig	1:1000	Synaptic Systems	258-104	AB_2661870
Tbr1	Rabbit	1:500	Millipore	AB10554	AB_10806888
Cux1	Rabbit	1:500	Santa Cruz Biotech	sc-13024	AB_2261231
NECAB1	Rabbit	1:2000	Sigma	HPA023629	AB1848014
NeuN	Mouse	1:250	Millipore	MAB377	AB_2298772
Somatostatin	Rabbit	1:2000	Peninsula Labs	T-4103	AB_518614
VGlut3	Rabbit	1:1000	Synaptic Systems	135-203	AB_887886
VIP	Rabbit	1:1000	ImmunoStar	20077	AB_572270
Vgat	Rabbit	1:500	Synaptic Systems	131-003	AB_887869
Vgat	Guinea Pig	1:500	Synaptic Systems	131-005	AB_1106810
Parvalbumin	Rabbit	1:1000	Swant	PV27	AB_2631173

Microscopy

Imaging was performed on either a Zeiss Axio Imager M2 fluorescence upright microscope equipped with an Apotome.2 module or a Zeiss LSM 980 laser scanning confocal build around a motorized Zeiss Axio Observer Z1 inverted microscope with a

Piezo stage. The Axio Imager M2 uses a metal halide light source (HXP 200 C), Axiocam 506 mono camera, and 10X/0.3 NA EC Plan-Neofluar, 20X/0.8 NA Plan-Apochromat objectives. The LSM 980 confocal light path has two multi-alkali PMTs and two GaAsP PMTs for four track imaging. Confocal images were acquired using a 63X/1.4 NA Plan-Apochromat Oil DIC M27 objective. Z-stack images were acquired and analyzed offline in ImageJ/FIJI[92] or Imaris 9.8 (Oxford Instruments). Images used for quantification between genotypes were acquired using the same exposure times. Brightness and contrast were adjusted in FIJI to improve visibility of images for publication. Figures were composed in Adobe Illustrator 2023 (Adobe Systems).

Image Quantification

For imaging experiments, 4-8 images were acquired from 2-4 coronal sections per animal, and at least three animals per genotype were used for analysis.

Cortical Lamination

Images of somatosensory cortex were acquired using a 10X objective on a Zeiss Axio Imager M2. 4µm z-stacks covering 16µm were acquired and multiple tiles were stitched together. Maximum projections were used for analysis. In FIJI, the straight line tool with a 300µm line width was used to measure the fluorescence profile from corpus callosum to pial surface. Background fluorescence was determined as the average fluorescence of the 20 darkest pixels; background was then subtracted from all points. The cortical distance was broken into 10 bins and average fluorescence within each bin was compared between genotypes.

Hippocampal CA1 CB_1R and PV Distribution

Images of dorsal hippocampus were acquired using a 20X objective on a Zeiss Axio Imager M2. Maximum projection images of 1.5µm z-stacks covering 20µm were analyzed in FIJI. The straight line tool with a 300µm line width was used to measure the fluorescence profile within SO, SP, and SR of CA1, avoiding Parvalbumin$^+$ cell bodies. Background fluorescence was determined as the average fluorescence of the 50 darkest pixels; background was then subtracted from all points. The thickness of SP was determined using Hoechst fluorescence. Average fluorescence within SO/SP/SR was compared between genotypes.

Hippocampal CB_1R/PV/VGAT Density and Co-localization

Images of dorsal hippocampus were acquired using a 63X objective on a Zeiss LSM 980. 3.2µm z-stacks covering 48µm were analyzed in Imaris. Hoechst fluorescence was used to determine the bounds of SP. The Imaris Spots function was used to determine the location of synaptic puncta in 3-dimensional space. Synaptic puncta were deemed to be co-localized if they were within 1µm of each other.

Western Blot

Cortex and hippocampus were dissected from P0 brains and solubilized in 1mL of lysis buffer containing 100mM NaCl, 50nM Tris, 2.5mM $CaCl_2$, 1% Triton X-100, 1% n-Octyl-β-D-glucopyranoside, and protease inhibitors. Lysate was incubated at 4°C for 1 hour and then spun at 12,500g for 25 minutes. Supernatant containing 3,000µg of protein (as determined by Pierce BCA Protein Assay) was applied to agarose-bound Wheat Germ Agglutinin (WGA) (Vector Labs) overnight at 4°C. Beads were washed 3X in TBS and boiled in 1X LDS sample buffer with 2-Mercaptoethanol (1:100) for 5 minutes. Samples

were run on a 4-15% gradient polyacrylamide gel at 100V for 75 minutes and then transferred to a PVDF membrane (100V for 100 minutes). For immunoblotting, membranes were blocked in 5% milk TBST and then incubated overnight at 4°C in 5% milk TBST containing primary antibody. Antibodies used: α-Dystroglycan (IIH6C4) (Millipore cat. no. 05-593, mouse IgM, 1:500), MANDAG2 (DSHB cat. no. 7D11, mouse IgG1, 1:500), β3-tubulin (Cell Signaling Technology cat. no. 5568, rabbit, 1:2000). Membranes were washed 3X in TBST and incubated on fluorescent IRDye secondary antibody (1:10,000, LI-COR) in 5% milk TBST for 1 hour at room temperature. Membranes were imaged using a LI-COR Odyssey CLx 0918 imager and signal analyzed using LI-COR Image Studio Lite version 5.2.

Electrophysiology

For acute slice preparation, mice were deeply anesthetized in 4% isoflurane and subsequently injected with a lethal dose of 2% 2, 2, 2-Tribromoethanol in sterile water followed by transcardial perfusion with 10mL ice cold cutting solution containing the following (in mM): 93 NMDG, 2.5 KCl, 1.2 NaH_2PO_4, 30 $NaHCO_3$, 20 HEPES, 24 glucose, 5 Na Ascorbate, 2 Thiourea, 3 Na Pyruvate, 13 N-Acetyl Cysteine, 1 Kynurenic acid, 10 $MgSO_4$, 0.5 $CaCl_2$; pH 7.3, 300-340mmol/kg. After rapid decapitation, the brain was briefly submerged in ice cold cut solution bubbled with carbogen (95% oxygen, 5% CO2) and then sectioned into 300µm sagittal sections (Leica VT1200S vibratome) in bubbled ice-cold cut solution. Slices were recovered in 37°C cut solution, bubbled, for 15 minutes followed by 1 hour in room temperature recording ACSF (containing, in mM:

125 NaCl, 25 $NaHCO_3$, 1.25 NaH_2PO_4, 3 KCl, 25 D-Glucose, 2 $CaCl_2$, 1 $MgCl_2$) with an osmolarity of 310-320mmol/kg and supplemented with 1.5mM Na Ascorbate, bubbled.

CA1 pyramidal cells were patched in whole cell configuration using 3-5MΩ borosilicate glass pipettes filled with high chloride internal solution containing the following (in mM): 125 CsCl, 2.5 $MgCl_2$, 0.5 EGTA, 10 HEPES, 2 Mg-ATP, 0.3 Na-GTP, 5 QX-314; pH 7.2, 300mmol/kg. Pipettes were wrapped in parafilm to reduce capacitive currents. Cells were voltage clamped at -70mV and continuously superfused with 2-3 mL/min bubbled recording ACSF (310-320mmol/kg) containing 10μM NBQX to block excitatory transmission. Recordings were performed at 34°C. After 5 minutes of spontaneous IPSC (sIPSC) recording, 10μM Carbachol was added to the perfusate and another 5 minutes of sIPSC were recorded. Signals were amplified with an AxoPatch 200B amplifier (Molecular Devices), low-pass filtered at 5 kHz, and digitized and sampled at 10 kHz with a NIDAQ analog-to-digital board (National Instruments). Data were acquired and analyzed using a custom script in Igor Pro 8 (Wavemetrics). A hyperpolarizing step of -10mV was applied before each sweep to monitor input resistance, series resistance, and measure cell capacitance. Series resistance was not compensated and was maintained below 20MΩ. Cells were excluded if series resistance changed by more than 25%.

To calculate the proportion of cells that responded to Carbachol, cells were sorted into “responsive” and “non-responsive” categories. Cells were categorized as responsive if sIPSC frequency increased by 20% or more with the addition of Carbachol. If sIPSC frequency in a cell changed by less than 20% or less than 0.5Hz it was deemed non-responsive.

Flurothyl Seizure Induction

Mice aged P40-P55 were used for the flurothyl-induced seizure susceptibility assay to determine seizure threshold. Briefly, mice were placed in an enclosed glass chamber equipped with a vaporization chamber out of reach of the mouse. Volatile liquid 10% Bis (2,2,2-Trifluorotheyl) Ether (Millipore Sigma cat. no 287571) in 95% EtOH was delivered to the vaporization chamber at a rate of 6mL/hour. Seizure latency was determined as the amount of time until generalized tonic-clonic seizure (TCS). Upon exhibiting TCS, animals were immediately removed from the chamber and returned to their home cage, whereupon seizures ceased rapidly. Sample size was determined using power analysis as described below. The *Emx1*^{Cre}*;Dag1* experimental groups were powered sufficiently to determine sex differences. Because no sex difference was found (**Supplementary Fig. 9C**), sexes were pooled for the remaining experiments. For statistical tests, outliers were excluded. Outliers were calculated as follows: first, the interquartile range (IQR) was calculated and multiplied by 1.5. This 1.5*IQR value was subtracted from the 25% quartile (Q1) and added to the 75% quartile (Q3). Points outside of the range Q1 - 1.5*IQR < x < Q3 + 1.5*IQR were categorized as outliers and indicated as such on all graphs. This was done to remove bias from extreme outliers observed in this experiment.

Statistical analysis

Phenotypic analyses were conducted using tissue collected from at least three mice per genotype from at least two independent litters. The number of mice and

replicates used for each analysis (“N”) are indicated in **Supplementary Table 1**. Power analysis using pilot data was used to determine samples sizes with $\alpha = 0.05$ and $\beta = 0.80$. Phenotypes were indistinguishable between male and female mice and were analyzed together. In many cases, highly penetrant phenotypes revealed the genotypes of the mice and no blinding could be performed. For comparisons between two groups, significance was determined using a two-tailed Students t-test. For comparisons between more than two groups, significance was determined using a 2-way ANOVA with Tukey HSD post-hoc analysis. Statistical significance was set at $\alpha = 0.05$ ($p < 0.05$) and data presented as means ± SEM. Statistical analyses and data visualization were performed in R (version 4.0.2).

DATA AVAILABILITY

The data that support the findings of this study are available from the corresponding author upon reasonable request.

REFERENCES

1. Colognato, H. *et al.* Identification of dystroglycan as a second laminin receptor in oligodendrocytes, with a role in myelination. *Development* **134**, 1723–1736 (2007).
2. Nickolls, A. R. & Bönnemann, C. G. The roles of dystroglycan in the nervous system: Insights from animal models of muscular dystrophy. *DMM Dis. Models Mech.* **11**, dmm035931 (2018).
3. Tian, M. *et al.* Dystroglycan in the cerebellum is a laminin α2-chain binding protein at the glial-vascular interface and is expressed in Purkinje cells. *Eur. J. Neurosci.* **8**, 2739–2747 (1996).
4. Zaccaria, M. L., Di Tommaso, F., Brancaccio, A., Paggi, P. & Petrucci, T. C. Dystroglycan distribution in adult mouse brain: A light and electron microscopy study. *Neuroscience* **104**, 311–324 (2001).
5. Nguyen, H. *et al.* Glial scaffold required for cerebellar granule cell migration is dependent on dystroglycan function as a receptor for basement membrane proteins. *Acta Neuropathol. Commun.* **2**, (2014).
6. Omori, Y. *et al.* Presynaptic dystroglycan-pikachurin complex regulates the proper synaptic connection between retinal photoreceptor and bipolar cells. *J. Neurosci.* **32**, 6126–6137 (2012).
7. Orlandi, C. *et al.* Transsynaptic Binding of Orphan Receptor GPR179 to Dystroglycan-Pikachurin Complex Is Essential for the Synaptic Organization of Photoreceptors. *Cell Rep.* **25**, 130-145.e5 (2018).

8. Briatore, F., Patrizi, A., Viltono, L., Sassoe-Pognetto, M. & Wulff, P. Quantitative organization of GABAergic synapses in the molecular layer of the mouse cerebellar cortex. *PLoS ONE* **5**, (2010).

9. Briatore, F. *et al.* Dystroglycan Mediates Clustering of Essential GABAergic Components in Cerebellar Purkinje Cells. *Front. Mol. Neurosci.* **13**, 164 (2020).

10. Patrizi, A. *et al.* Synapse formation and clustering of neuroligin-2 in the absence of GABAA receptors. *Proc. Natl. Acad. Sci.* **105**, 13151–13156 (2008).

11. Brünig, I., Suter, A., Knuesel, I., Lüscher, B. & Fritschy, J. M. GABAergic Terminals Are Required for Postsynaptic Clustering of Dystrophin but Not of GABAA Receptors and Gephyrin. *J. Neurosci.* **22**, 4805–4813 (2002).

12. Lévi, S. *et al.* Dystroglycan Is Selectively Associated with Inhibitory GABAergic Synapses but Is Dispensable for Their Differentiation. *J. Neurosci.* **22**, 4274–4285 (2002).

13. Ervasti, J. M. & Campbell, K. P. Membrane organization of the dystrophin-glycoprotein complex. *Cell* **66**, 1121–1131 (1991).

14. Holt, K. H., Crosbie, R. H., Venzke, D. P. & Campbell, K. P. Biosynthesis of dystroglycan: Processing of a precursor propeptide. *FEBS Lett.* **468**, 79–83 (2000).

15. Ibraghimov-Beskrovnaya, O. *et al.* Primary structure of dystrophin-associated glycoproteins linking dystrophin to the extracellular matrix. *Nature* **355**, 696–702 (1992).

16. Moore, C. J. & Winder, S. J. Dystroglycan versatility in cell adhesion: A tale of multiple motifs. *Cell Commun. Signal.* **8**, 3 (2010).

17. Jahncke, J. N. & Wright, K. M. The many roles of dystroglycan in nervous system development and function. *Dev. Dyn.* **252**, 61–80 (2023).

18. Blaeser, A. *et al.* Mouse models of fukutin-related protein mutations show a wide range of disease phenotypes. *Hum. Genet.* **132**, 923–934 (2013).

19. Barresi, R. & Campbell, K. P. Dystroglycan: From biosynthesis to pathogenesis of human disease. *J. Cell Sci.* **119**, 199–207 (2006).

20. Muntoni, F., Torelli, S., Wells, D. J. & Brown, S. C. Muscular dystrophies due to glycosylation defects: diagnosis and therapeutic strategies. *Curr. Opin. Neurol.* **24**, 437–442 (2011).

21. Taniguchi-Ikeda, M., Morioka, I., Iijima, K. & Toda, T. Mechanistic aspects of the formation of α-dystroglycan and therapeutic research for the treatment of α-dystroglycanopathy: A review. *Mol. Aspects Med.* **51**, 115–124 (2016).

22. Godfrey, C. *et al.* Refining genotype–phenotype correlations in muscular dystrophies with defective glycosylation of dystroglycan. *Brain* **130**, 2725–2735 (2007).

23. Clement, E. *et al.* Brain involvement in muscular dystrophies with defective dystroglycan glycosylation. *Ann. Neurol.* **64**, 573–582 (2008).

24. Myshrall, T. D. *et al.* Dystroglycan on radial glia end feet is required for pial basement membrane integrity and columnar organization of the developing cerebral cortex. *J. Neuropathol. Exp. Neurol.* **71**, 1047–1063 (2012).

25. Satz, J. S. *et al.* Brain and eye malformations resembling Walker-Warburg syndrome are recapitulated in mice by dystroglycan deletion in the epiblast. *J. Neurosci.* **28**, 10567–10575 (2008).

26. Satz, J. S. *et al.* Distinct functions of glial and neuronal dystroglycan in the developing and adult mouse brain. *J. Neurosci.* **30**, 14560–14572 (2010).

27. Früh, S. *et al.* Neuronal dystroglycan is necessary for formation and maintenance of functional CCK-positive basket cell terminals on pyramidal cells. *J. Neurosci.* **36**, 10296–10313 (2016).

28. Miller, D. S. & Wright, K. M. Neuronal Dystroglycan regulates postnatal development of CCK/cannabinoid receptor-1 interneurons. *Neural Develop.* **16**, (2021).

29. Liang, H., Hippenmeyer, S. & Ghashghaei, H. T. A Nestin-cre transgenic mouse is insufficient for recombination in early embryonic neural progenitors. *Biol. Open* **1**, 1200–1203 (2012).

30. Manya, H. *et al.* Demonstration of mammalian protein O-mannosyltransferase activity: Coexpression of POMT1 and POMT2 required for enzymatic activity. *Proc. Natl. Acad. Sci.* **101**, 500–505 (2004).

31. Hu, H., Liu, Y., Bampoe, K., He, Y. & Yu, M. Postnatal Gene Therapy Improves Spatial Learning Despite the Presence of Neuronal Ectopia in a Model of Neuronal Migration Disorder. *Genes* **7**, 105 (2016).

32. Reeuwijk, J. van *et al.* POMT2 mutations cause α-dystroglycan hypoglycosylation and Walker-Warburg syndrome. *J. Med. Genet.* **42**, 907–912 (2005).

33. Yanagisawa, A. *et al.* New POMT2 mutations causing congenital muscular dystrophy: Identification of a founder mutation. *Neurology* **69**, 1254–1260 (2007).

34. Lindenmaier, L. B., Parmentier, N., Guo, C., Tissir, F. & Wright, K. M. Dystroglycan is a scaffold for extracellular axon guidance decisions. *eLife* **8**, (2019).

35. Satz, J. S. *et al.* Visual impairment in the absence of dystroglycan. *J. Neurosci.* **29**, 13136–13146 (2009).

36. Wright, K. M. *et al.* Dystroglycan Organizes Axon Guidance Cue Localization and Axonal Pathfinding. *Neuron* **76**, 931–944 (2012).

37. Brockington, M. *et al.* Mutations in the Fukutin-Related Protein Gene (FKRP) Cause a Form of Congenital Muscular Dystrophy with Secondary Laminin α2 Deficiency and Abnormal Glycosylation of α-Dystroglycan. *Am. J. Hum. Genet.* **69**, 1198–1209 (2001).

38. Yoshida-Moriguchi, T. & Campbell, K. P. Matriglycan: a novel polysaccharide that links dystroglycan to the basement membrane. *Glycobiology* **25**, 702–713 (2015).

39. Sheikh, M. O. *et al.* Cell surface glycan engineering reveals that matriglycan alone can recapitulate dystroglycan binding and function. *Nat. Commun.* **13**, 3617 (2022).

40. Durbeej, M., Henry, M. D., Ferletta, M., Campbell, K. P. & Ekblom, P. Distribution of dystroglycan in normal adult mouse tissues. *J. Histochem. Cytochem.* **46**, 449–457 (1998).

41. Moore, S. A. *et al.* Deletion of brain dystroglycan recapitulates aspects of congenital muscular dystrophy. *Nature* **418**, 422–425 (2002).

42. Pawlisz, A. S. & Feng, Y. Three-dimensional regulation of radial glial functions by lis1-nde1 and dystrophin glycoprotein complexes. *PLoS Biol.* **9**, (2011).

43. Hu, H. *et al.* Conditional knockout of protein O-mannosyltransferase 2 reveals tissue-specific roles of O-mannosyl glycosylation in brain development. *J. Comp. Neurol.* **519**, 1320–1337 (2011).

44. Chan, Y. M. *et al.* Fukutin-related protein is essential for mouse muscle, brain and eye development and mutation recapitulates the wide clinical spectrums of dystroglycanopathies. *Hum. Mol. Genet.* **19**, 3995–4006 (2010).

45. Holzfeind, P. J. *et al.* Skeletal, cardiac and tongue muscle pathology, defective retinal transmission, and neuronal migration defects in the Largemyd mouse defines a natural model for glycosylation-deficient muscle – eye – brain disorders. *Hum. Mol. Genet.* **11**, 2673–2687 (2002).

46. Monory, K., Polack, M., Remus, A., Lutz, B. & Korte, M. Cannabinoid CB1 Receptor Calibrates Excitatory Synaptic Balance in the Mouse Hippocampus. *J. Neurosci.* **35**, 3842–3850 (2015).

47. Katona, I. *et al.* Distribution of CB1 cannabinoid receptors in the amygdala and their role in the control of GABAergic transmission. *J. Neurosci. Off. J. Soc. Neurosci.* **21**, 9506–9518 (2001).

48. Földy, C., Neu, A., Jones, M. V. & Soltesz, I. Presynaptic, activity-dependent modulation of cannabinoid type 1 receptor-mediated inhibition of GABA release. *J. Neurosci. Off. J. Soc. Neurosci.* **26**, 1465–1469 (2006).

49. Morozov, Y. M. & Freund, T. F. Postnatal development and migration of cholecystokinin-immunoreactive interneurons in rat hippocampus. *Neuroscience* **120**, 923–939 (2003).

50. Morozov, Y. M. & Freund, T. F. Post-natal development of type 1 cannabinoid receptor immunoreactivity in the rat hippocampus. *Eur. J. Neurosci.* **18**, 1213–1222 (2003).

51. Morozov, Y. M., Torii, M. & Rakic, P. Origin, Early Commitment, Migratory Routes, and Destination of Cannabinoid Type 1 Receptor-Containing Interneurons. *Cereb. Cortex* **19**, i78–i89 (2009).

52. Berghuis, P. *et al.* Hardwiring the brain: endocannabinoids shape neuronal connectivity. *Science* **316**, 1212–1216 (2007).

53. Eggan, S. M., Mizoguchi, Y., Stoyak, S. R. & Lewis, D. A. Development of Cannabinoid 1 Receptor Protein and Messenger RNA in Monkey Dorsolateral Prefrontal Cortex. *Cereb. Cortex* **20**, 1164–1174 (2010).

54. Mulder, J. *et al.* Endocannabinoid signaling controls pyramidal cell specification and long-range axon patterning. *Proc. Natl. Acad. Sci.* **105**, 8760–8765 (2008).

55. Vitalis, T. *et al.* The type 1 cannabinoid receptor is highly expressed in embryonic cortical projection neurons and negatively regulates neurite growth in vitro. *Eur. J. Neurosci.* **28**, 1705–1718 (2008).

56. Freund, T. F. & Katona, I. Perisomatic inhibition. *Neuron* **56**, 33–42 (2007).

57. Nagode, D. A., Tang, A.-H., Yang, K. & Alger, B. E. Optogenetic identification of an intrinsic cholinergically driven inhibitory oscillator sensitive to cannabinoids and opioids in hippocampal CA1. *J. Physiol.* **592**, 103–123 (2014).

58. Yang, H. *et al.* Seizures and EEG characteristics in a cohort of pediatric patients with dystroglycanopathies. *Seizure* **101**, 39–47 (2022).

59. Dhaibani, M. A. A., El-Hattab, A. W., Ismayl, O. & Suleiman, J. B3GALNT2-Related Dystroglycanopathy: Expansion of the Phenotype with Novel Mutation Associated with Muscle-Eye-Brain Disease, Walker–Warburg Syndrome, Epileptic

Encephalopathy-West Syndrome, and Sensorineural Hearing Loss. *Neuropediatrics* **49**, 289–295 (2018).

60. Di Rosa, G. *et al.* A new form of alpha-dystroglycanopathy associated with severe drug-resistant epilepsy and unusual EEG features. *Epileptic. Disord.* **13**, 259–262 (2011).

61. Raphael, A. R. *et al.* Congenital Muscular Dystrophy and Generalized Epilepsy Caused by GMPPB Mutations. *Brain Res.* **0**, 66–71 (2014).

62. Egawa, K. *et al.* Flurothyl-induced seizure paradigm revealed higher seizure susceptibility in middle-aged Angelman syndrome mouse model. *Brain Dev.* **43**, 515–520 (2021).

63. Südhof, T. C. Towards an Understanding of Synapse Formation. *Neuron* **100**, 276–293 (2018).

64. Favuzzi, E. *et al.* Distinct molecular programs regulate synapse specificity in cortical inhibitory circuits. *Science* **363**, 413–417 (2019).

65. Sugita, S. *et al.* A stoichiometric complex of neurexins and dystroglycan in brain. *J. Cell Biol.* **154**, 435–445 (2001).

66. Fuccillo, M. V. *et al.* Single-Cell mRNA Profiling Reveals Cell-Type-Specific Expression of Neurexin Isoforms. *Neuron* **87**, 326–340 (2015).

67. Boucard, A. A., Chubykin, A. A., Comoletti, D., Taylor, P. & Südhof, T. C. A Splice Code for trans-Synaptic Cell Adhesion Mediated by Binding of Neuroligin 1 to α- and β-Neurexins. *Neuron* **48**, 229–236 (2005).

68. Reissner, C. *et al.* Dystroglycan binding to α-Neurexin competes with neurexophilin-1 and neuroligin in the brain. *J. Biol. Chem.* **289**, 27585–27603 (2014).

69. Ullrich, B., Ushkaryov, Y. A. & Südhof, T. C. Cartography of neurexins: More than 1000 isoforms generated by alternative splicing and expressed in distinct subsets of neurons. *Neuron* **14**, 497–507 (1995).

70. Trotter, J. H., Wang, C. Y., Zhou, P. & Südhof, T. C. A combinatorial code of neurexin-3 alternative splicing controls inhibitory synapses via a trans-synaptic dystroglycan signaling loop. 2022.05.09.491206 Preprint at https://doi.org/10.1101/2022.05.09.491206 (2022).

71. Chen, L. Y., Jiang, M., Zhang, B., Gokce, O. & Südhof, T. C. Conditional Deletion of All Neurexins Defines Diversity of Essential Synaptic Organizer Functions for Neurexins. *Neuron* **94**, 611-625.e4 (2017).

72. Dudanova, I., Tabuchi, K., Rohlmann, A., Südhof, T. C. & Missler, M. Deletion of α-neurexins does not cause a major impairment of axonal pathfinding or synapse formation. *J. Comp. Neurol.* **502**, 261–274 (2007).

73. Missler, M. *et al.* α-Neurexins couple Ca2+ channels to synaptic vesicle exocytosis. *Nature* **423**, 939–948 (2003).

74. Lin, P.-Y. *et al.* Neurexin-2: An inhibitory neurexin that restricts excitatory synapse formation in the hippocampus. *Sci. Adv.* **9**, eadd8856 (2023).

75. Knuesel, I. *et al.* Altered synaptic clustering of GABAA receptors in mice lacking dystrophin (mdx mice). *Eur. J. Neurosci.* **11**, 4457–4462 (1999).

76. Jagadha, V. & Becker, L. E. Brain morphology in Duchenne muscular dystrophy: A Golgi study. *Pediatr. Neurol.* **4**, 87–92 (1988).

77. Moizard, M.-P. *et al.* Severe cognitive impairment in DMD: obvious clinical evidence for Dp71 isoform point mutations screening. *Eur. J. Hum. Genet.* **8**, 552–556 (2000).

78. Naidoo, M. & Anthony, K. Dystrophin Dp71 and the Neuropathophysiology of Duchenne Muscular Dystrophy. *Mol. Neurobiol.* **57**, 1748–1767 (2020).

79. Krasowska, E., Zabłocki, K., Górecki, D. C. & Swinny, J. D. Aberrant location of inhibitory synaptic marker proteins in the hippocampus of dystrophin-deficient mice: Implications for cognitive impairment in Duchenne muscular dystrophy. *PLoS ONE* **9**, e108364 (2014).

80. Uezu, A. *et al.* Essential role for insyn1 in dystroglycan complex integrity and cognitive behaviors in mice. *eLife* **8**, (2019).

81. Meilleur, K. G. *et al.* Clinical, pathologic, and mutational spectrum of dystroglycanopathy caused by LARGE mutations. *J. Neuropathol. Exp. Neurol.* **73**, 425–441 (2014).

82. Mercuri, E. *et al.* Congenital muscular dystrophies with defective glycosylation of dystroglycan: A population study. *Neurology* **72**, 1802–1809 (2009).

83. Wang, J. *et al.* Epilepsy-associated genes. *Seizure* **44**, 11–20 (2017).

84. Kadiyala, S. B. *et al.* Eight Flurothyl-Induced Generalized Seizures Lead to the Rapid Evolution of Spontaneous Seizures in Mice: A Model of Epileptogenesis with Seizure Remission. *J. Neurosci.* **36**, 7485–7496 (2016).

85. Gu, B. *et al.* Ictal neural oscillatory alterations precede sudden unexpected death in epilepsy. *Brain Commun.* **4**, fcac073 (2022).

86. Kanagawa, M. Dystroglycanopathy: From Elucidation of Molecular and Pathological Mechanisms to Development of Treatment Methods. *Int. J. Mol. Sci.* **22**, 13162 (2021).

87. Cataldi, M. P., Lu, P., Blaeser, A. & Lu, Q. L. Ribitol restores functionally glycosylated α-dystroglycan and improves muscle function in dystrophic FKRP-mutant mice. *Nat. Commun.* **9**, 3448 (2018).

88. Cataldi, M. P., Blaeser, A., Lu, P., Leroy, V. & Lu, Q. L. ISPD Overexpression Enhances Ribitol-Induced Glycosylation of α-Dystroglycan in Dystrophic FKRP Mutant Mice. *Mol. Ther. - Methods Clin. Dev.* **17**, 271–280 (2020).

89. Cohn, R. D. *et al.* Disruption of Dag1 in differentiated skeletal muscle reveals a role for dystroglycan in muscle regeneration. *Cell* **110**, 639–648 (2002).

90. Peron, S. P., Freeman, J., Iyer, V., Guo, C. & Svoboda, K. A Cellular Resolution Map of Barrel Cortex Activity during Tactile Behavior. *Neuron* **86**, 783–799 (2015).

91. Gorski, J. A. *et al.* Cortical Excitatory Neurons and Glia, But Not GABAergic Neurons, Are Produced in the Emx1-Expressing Lineage. *J. Neurosci.* **22**, 6309–6314 (2002).

92. Schindelin, J. *et al.* Fiji: an open-source platform for biological-image analysis. *Nat. Methods* **9**, 676–682 (2012).

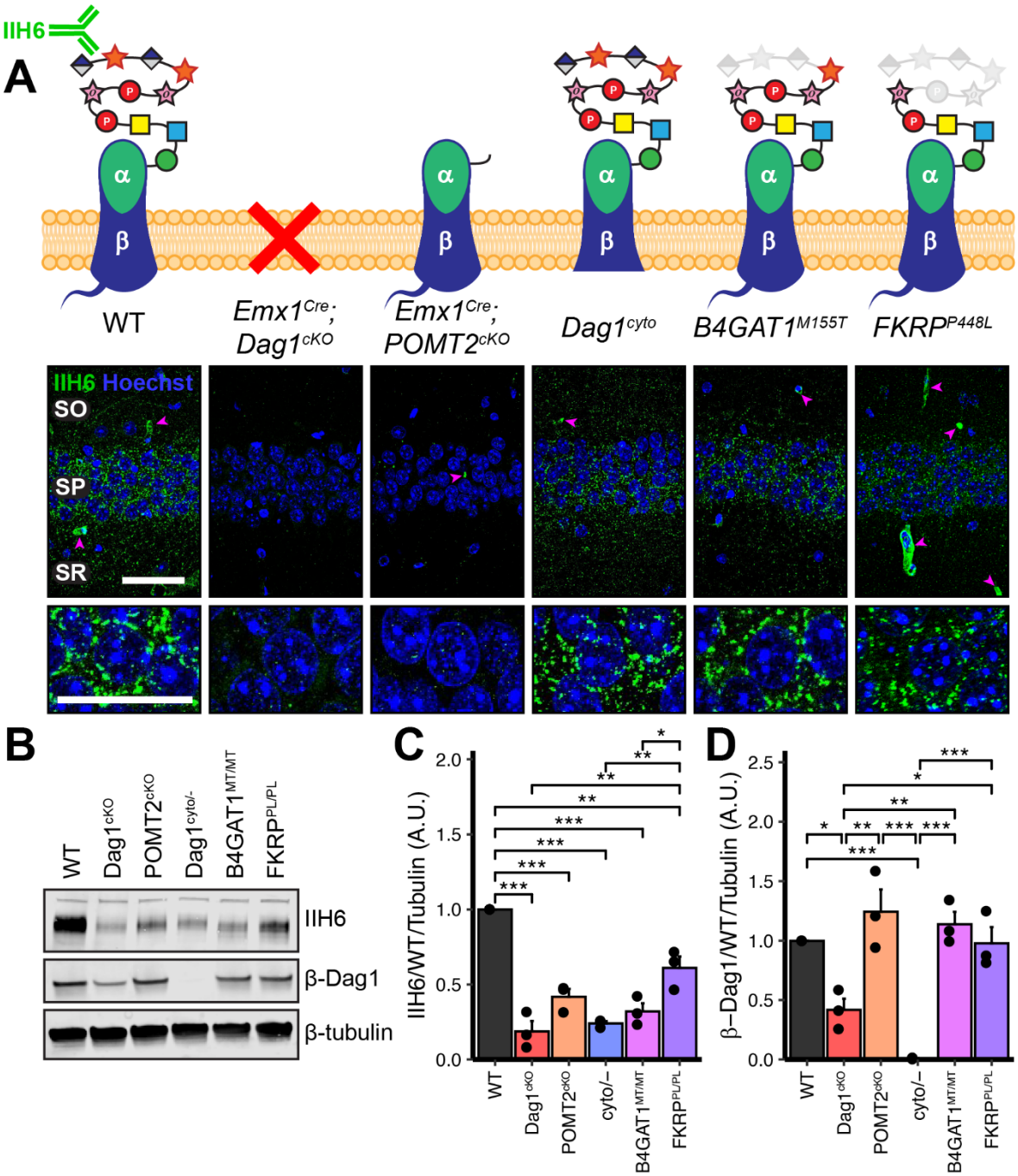

Figure 1. Dystroglycan synaptic localization and glycosylation in mouse models of dystroglycanopathy. (A) Schematic depiction of Dystroglycan in different mouse models. The IIH6 antibody recognizes the matriglycan repeats on extracellular αDag1. Hippocampal CA1 of P30 mice immunostained for Dystroglycan glycosylation (IIH6, green) and nuclear marker Hoechst (blue) show puncta of glycosylated Dystroglycan localized to the perisomatic region of pyramidal cells and to blood vessels (magenta arrowheads); scale bar = 50µm. Lower panels show cell bodies in SP; scale bar = 25µm. CA1 layers: SO, *stratum oriens*; SP, *stratum pyramidale*; SR, *stratum radiatum*.

(B) WGA-enriched lysates from P0 forebrain were immunoblotted for IIH6, β-Dag1, and β-tubulin. **(C-D)** Quantification of immunoblot in **(B)**. Error bars show mean + SEM.

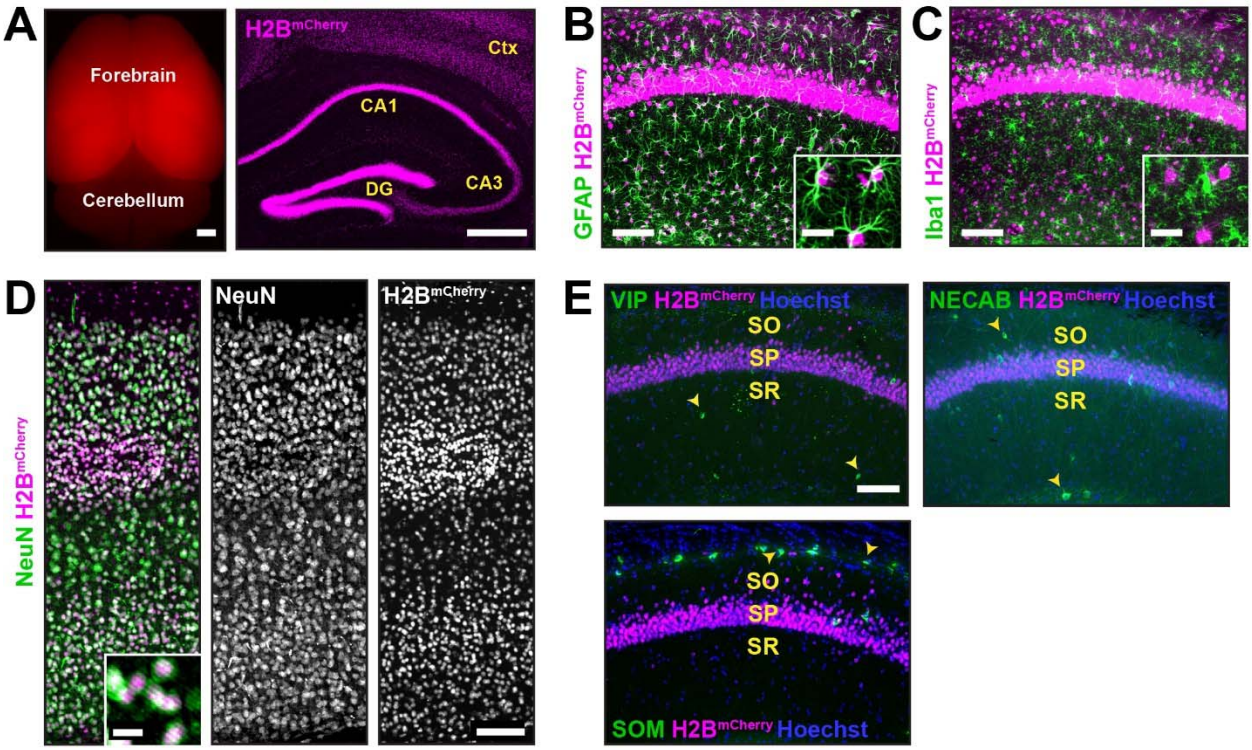

Supplementary Figure 1. *Emx1^{Cre}* drives recombination in forebrain excitatory neurons and astrocytes, but not interneurons or microglia. (A) Left; endogenous red fluorescence in the forebrain of P60 *Emx1^{Cre}*;*R26$^{LSL\text{-}H2B\text{-}mCherry}$* reporter mice (scale bar = 1mm). Right; coronal section of the forebrain from *Emx1^{Cre}*;*R26$^{LSL\text{-}H2B\text{-}mCherry}$* mice showing robust nuclear mCherry signal (magenta) in the cortex and hippocampus (scale bar = 500µm). **(B-E)** mCherry^{+} nuclei shown with markers of multiple cell types in the brain including astrocytes (GFAP, green) **(B)**, microglia (Iba1, green) **(C)**, and neurons (NeuN, green) **(D)** (scale bar = 100µm). Insets show enlarged images of mCherry^{+} nuclei with cell type markers (scale bar = 20µm). **(E)** mCherry^{+} nuclei with markers for different interneuron subtype markers (yellow arrowheads) (scale bar = 100µm) (VIP = Vasoactive intestinal peptide, NECAB = Neuronal calcium-binding protein 1, SOM = Somatostatin). *CA1 layers: SO, stratum oriens; SP, stratum pyramidale; SR, stratum radiatum.*

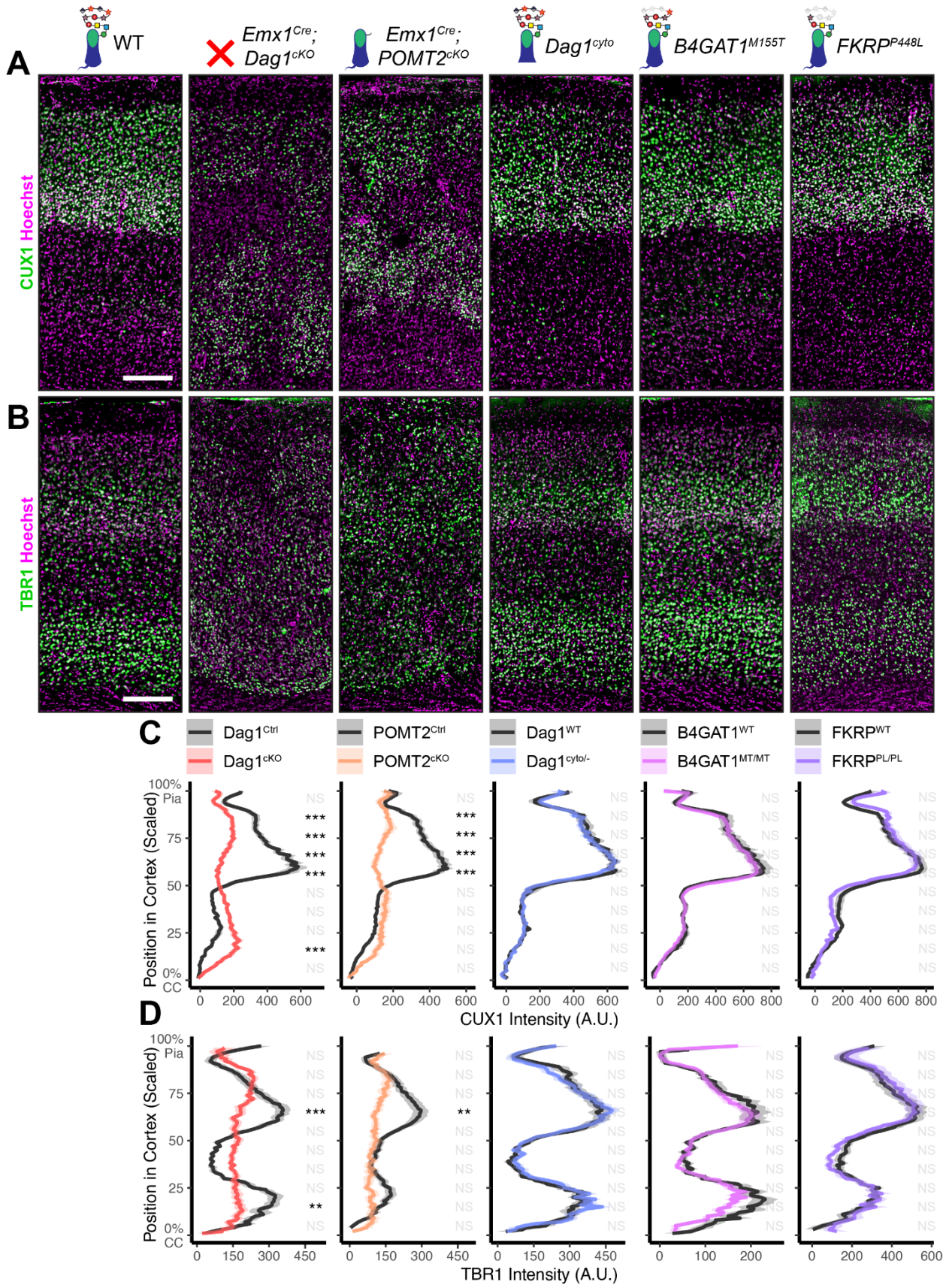
A
WT
Emx1Cre; Dag1cKO
Emx1Cre; POMT2cKO
Dag1cyto
B4GAT1M155T
FKRPP448L
CUX1 Hoechst
B
TBR1 Hoechst
C
Dag1Ctrl
Dag1cKO
POMT2Ctrl
POMT2cKO
Dag1WT
Dag1cyto/-
B4GAT1WT
B4GAT1MT/MT
FKRPWT
FKRPPL/PL
Position in Cortex (Scaled)
100% Pia
75
50
25
0% CC
CUX1 Intensity (A.U.)
D
TBR1 Intensity (A.U.)

Figure 2. Dystroglycan is required for cortical neuron migration in a glycosylation-dependent manner and independent of intracellular interactions. Immunostaining for cortical layer markers **(A)** CUX1 (layers 2-4) and **(B)** TBR1 (layers 3 and 6) in P30 somatosensory cortex (scale bar = 200μm). Layer markers are shown in green. Nuclear marker Hoechst is shown in magenta. Quantification of fluorescence intensity of layer markers shown for **(C)** CUX1 and **(D)** TBR1**.** Shaded regions of intensity profile illustrate ± SEM. See **Supplementary Table 1** for Ns. *Significance: * = $p < 0.05$, ** = $p < 0.01$, *** = $p < 0.001$, NS = $p \geq 0.05$. Abbreviations: CC, corpus callosum; A.U., arbitrary units.*

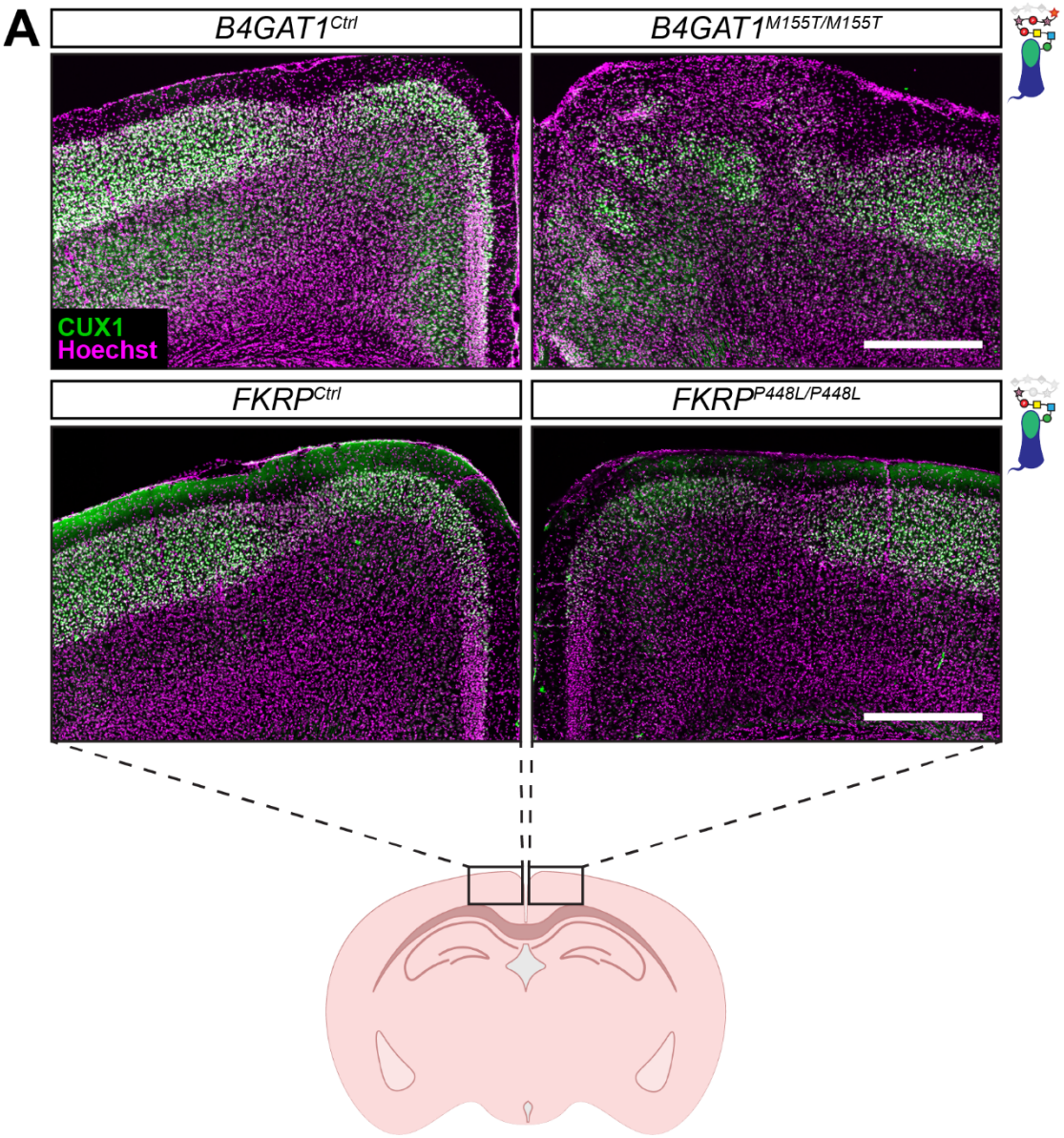

Supplementary Figure 2. Cortical migration is disrupted at midline of *B4GAT1*$^{M155T/M155T}$ but not *FKRP*$^{P448L/P448L}$ mutants. (A) Immunostaining for cortical layer marker CUX1 (layers 2-4) in P30 somatosensory cortex (scale bar = 500µm). CUX1 is shown in green. Nuclear marker Hoechst is shown in magenta. Cortical migration is normal in both *B4GAT1* and *FKRP* point mutants except at midline, where the *B4GAT1* mutants show a migration phenotype not seen in the *FKRP* point mutants. This phenotype was observed with 100% penetrance in the *B4GAT1* mutants and 0% in the *FKRP* mutants.

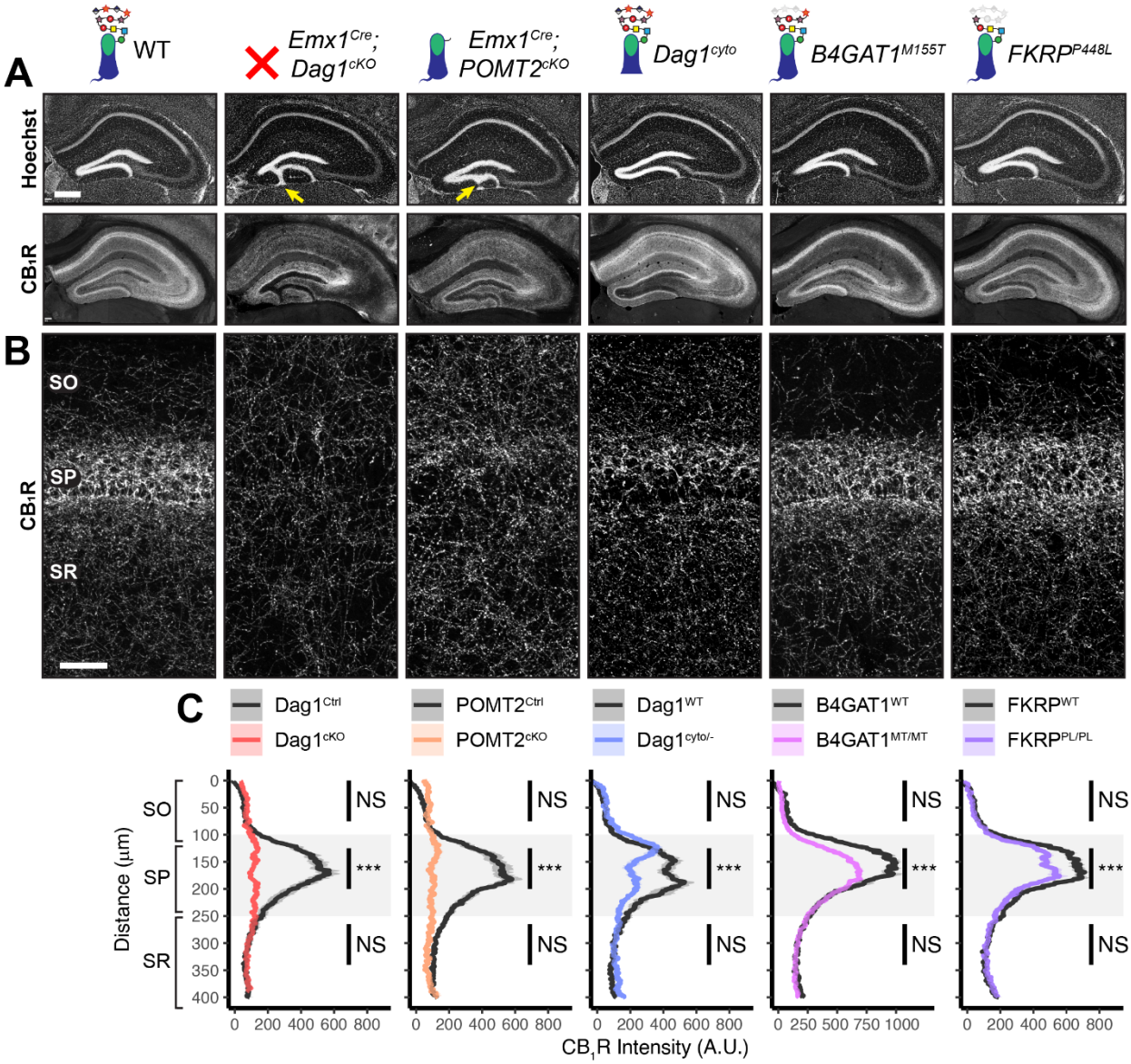

Figure 3. *Dag1* is required for CCK$^+$/CB$_1$R$^+$ basket IN perisomatic axon targeting in *stratum pyramidale* of hippocampal CA1-3. (A) Nuclear marker Hoechst (upper panels) shows hippocampal morphology. Granule cell migration is disrupted in dentate gyrus of *Emx1^{Cre};Dag1^{cKOs}* and *Emx1^{Cre};POMT2^{cKOs}* (yellow arrows). CA1-3 gross morphology is normal in all models. CB$_1$R immunostaining (lower panels) shows abnormal CCK$^+$/CB$_1$R$^+$ basket interneuron targeting in CA1-3 to varying degrees across models (scale bar = 400µm). **(B)** Higher magnification view of CB$_1$R immunostaining in CA1 (scale bar = 50µm). **(C)** Quantification of CA1 CB$_1$R fluorescence intensity profile. Shaded regions of intensity profile illustrate ± SEM. Gray region highlights SP. See **Supplementary Table 1** for Ns. *Significance: * = $p < 0.05$, ** = $p < 0.01$, *** = $p < 0.001$, NS = $p \geq 0.05$. Abbreviations: A.U., arbitrary units; SO, stratum oriens; SP, stratum pyramidale; SR, stratum radiatum.*

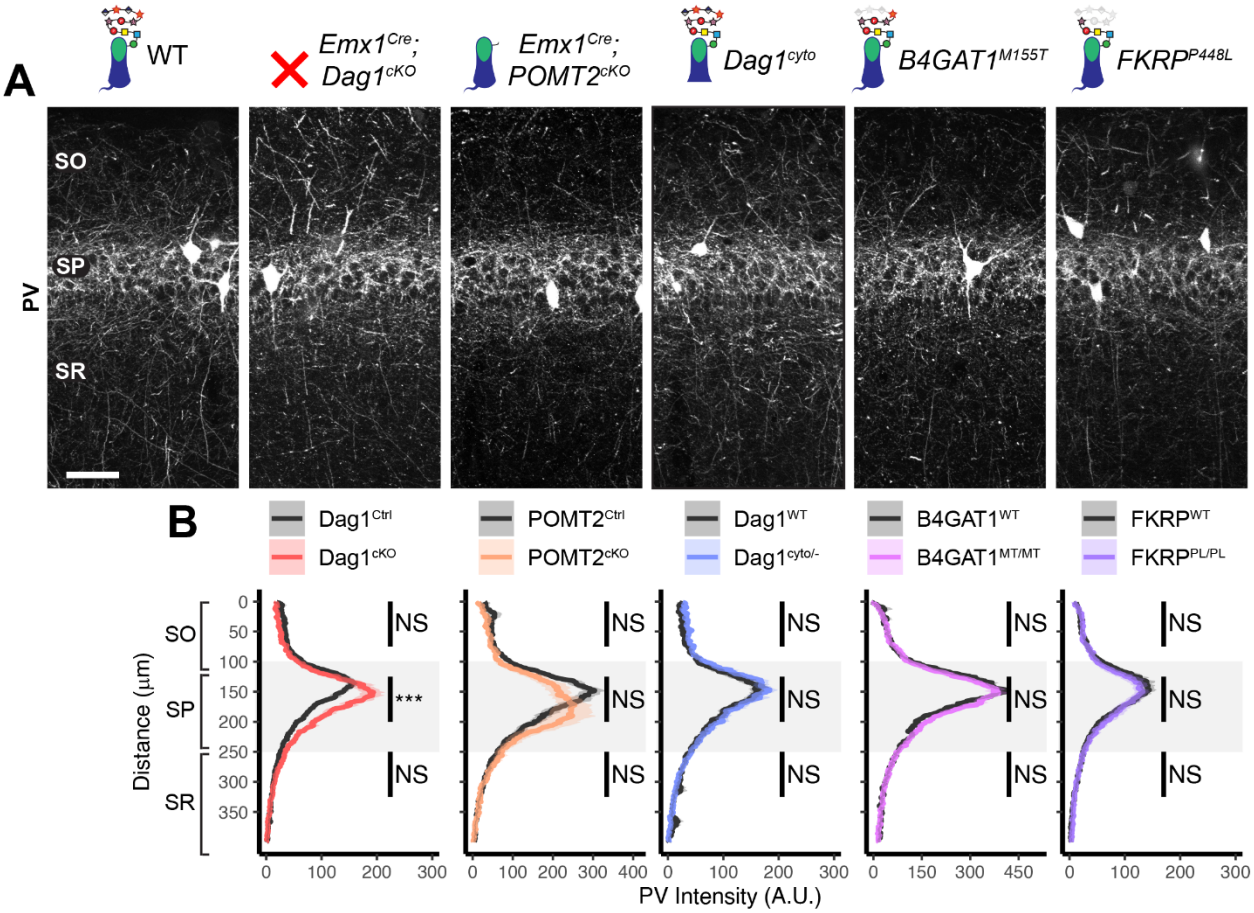

Supplementary Figure 3. Parvalbumin$^+$ basket INs do not require *Dag1* for proper axon targeting in hippocampal CA1. (A) Parvalbumin (PV) immunostaining in P30 hippocampal CA1 shows that PV$^+$ basket interneurons exhibit normal distribution in CA1 for all genetic models except for an increase in PV intensity within *stratum pyramidale* of *Emx1^{Cre};Dag1^{cKOs}* (scale bar = 50µm). **(B)** Quantification of CA1 PV fluorescence intensity profile. Shaded regions of intensity profile illustrate ± SEM. Gray region highlights SP. See **Supplementary Table 1** for Ns. *Significance: * = p < 0.05, ** = p < 0.01, *** = p < 0.001, NS = p ≥ 0.05. Abbreviations: A.U., arbitrary units; SO, stratum oriens; SP, stratum pyramidale; SR, stratum radiatum.*

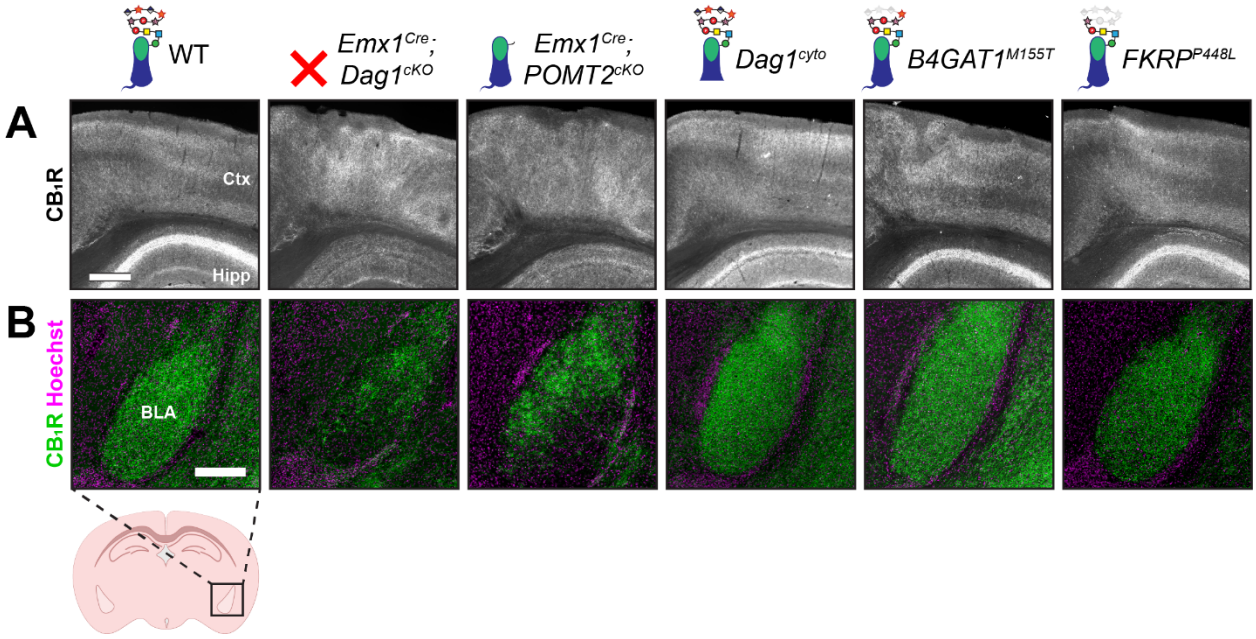

Supplementary Figure 4. Altered CB_1R expression in cortex and basolateral amygdala of *Dag1* and *POMT2* mutants. (A) CB_1R immunostaining in P30 coronal sections showing somatosensory cortex (Ctx) and CA1 of hippocampus (Hipp) (scale bar = 400µm). **(B)** CB_1R immunostaining (green) shown with nuclear marker Hoechst (magenta) in basolateral amygdala (BLA) (scale bar = 250µm).

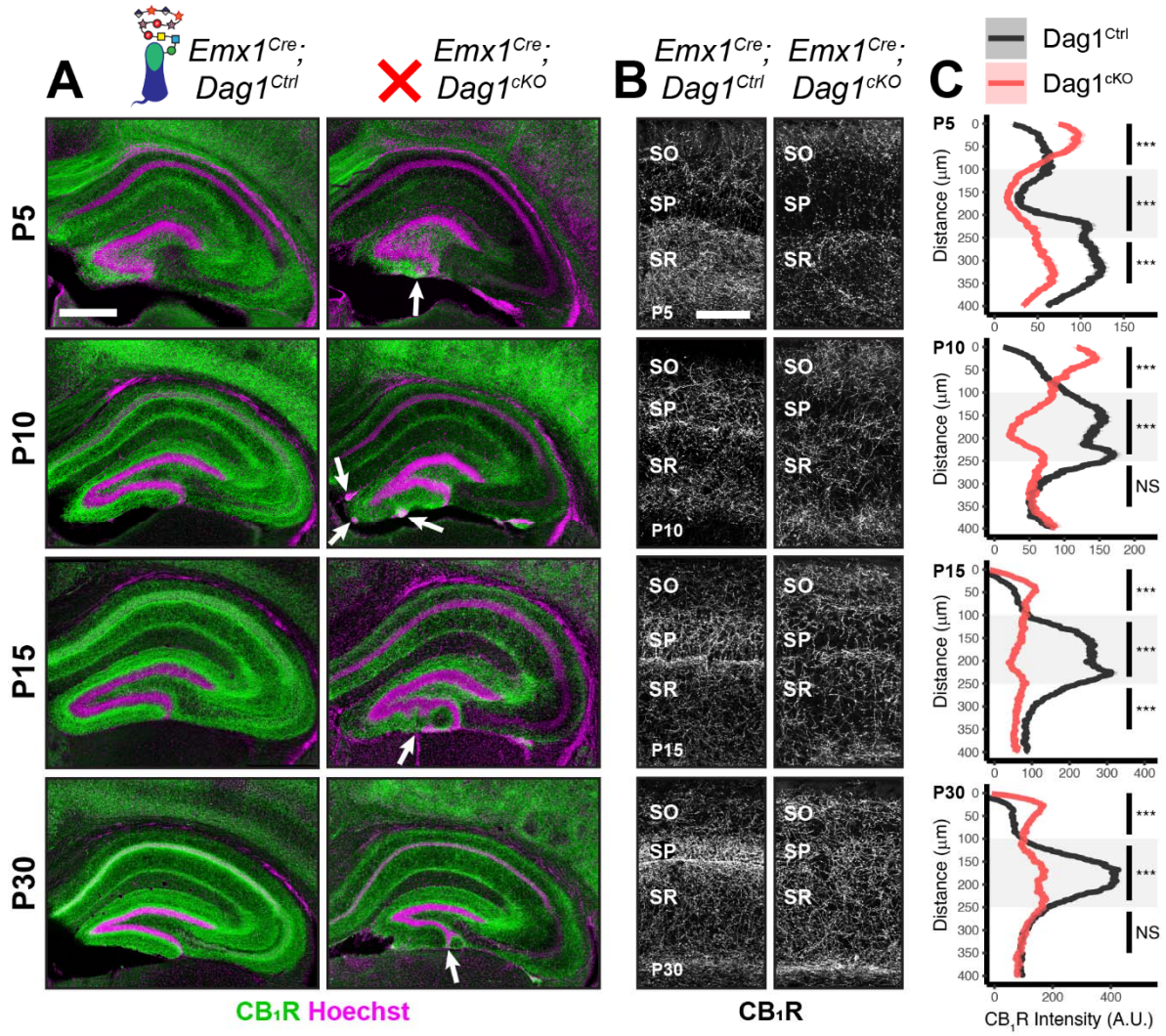

Figure 4. *Dag1* is required for CCK$^+$/CB$_1$R$^+$ IN axon targeting during early postnatal development. (A) Immunostaining for CB$_1$R$^+$ axon terminals (green) in the hippocampus of *Emx1^{Cre};Dag1* controls (left) and cKOs (right) at ages P5-P30. Nuclear marker Hoechst is shown in magenta. White arrowheads indicate migration errors in dentate granule cells *Emx1^{Cre};Dag1^{cKO}* mice. Scale bar = 500µm. **(B)** Higher magnification images of CB$_1$R$^+$ axon terminals in CA1 of *Emx1^{Cre};Dag1* controls (left) and cKOs (right) at ages P5-P30. Scale bar = 100µm. **(C)** Quantification of CB$_1$R fluorescence intensity profile in CA1. Shaded regions of intensity profile illustrate ± SEM. Gray region highlights SP. See **Supplementary Table 1** for Ns. *Significance: * = $p < 0.05$, ** = $p < 0.01$, *** = $p < 0.001$, NS = $p \geq 0.05$. Abbreviations: A.U., arbitrary units; SO, stratum oriens; SP, stratum pyramidale; SR, stratum radiatum.*

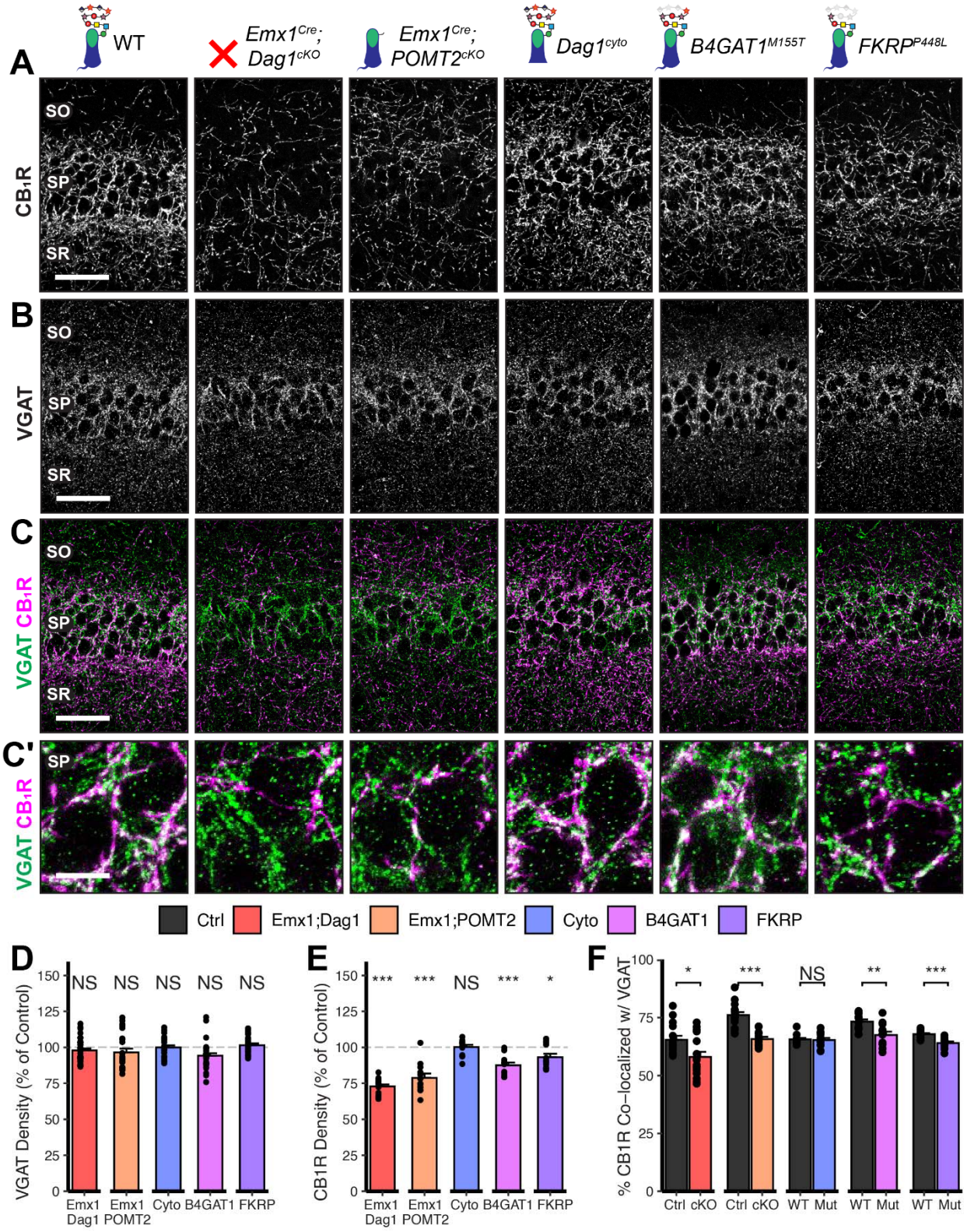

Figure 5. *Dag1* and *POMT2* cKOs exhibit impaired CB1R$^+$ basket synapse formation in *stratum pyramidale* of hippocampal CA1. P30 coronal sections

immunostained for **(A)** CB_1R and **(B)** VGAT in hippocampal CA1; merged image in **(C)** shows CB_1R in magenta and VGAT in green. (A-C) Scale bar = 50µm. (Higher magnification view of SP in **(C')**; scale bar = 10µm.) **(D)** Quantification of VGAT puncta density in SP expressed as a percent of control. **(E)** Quantification of CB_1R puncta density in SP expressed as a percent of control. **(F)** Quantification of co-localization between VGAT and CB_1R in SP to estimate putative CB_1R^+ basket cell synapse formation. Error bars show mean + SEM. (For quantification of puncta densities and co-localization in SO and SR see **Supplementary Fig. 5**.) See **Supplementary Table 1** for Ns. *Significance: * = $p < 0.05$, ** = $p < 0.01$, *** = $p < 0.001$, NS = $p \geq 0.05$.*
Abbreviations: SO, stratum oriens; SP, stratum pyramidale; SR, stratum radiatum.

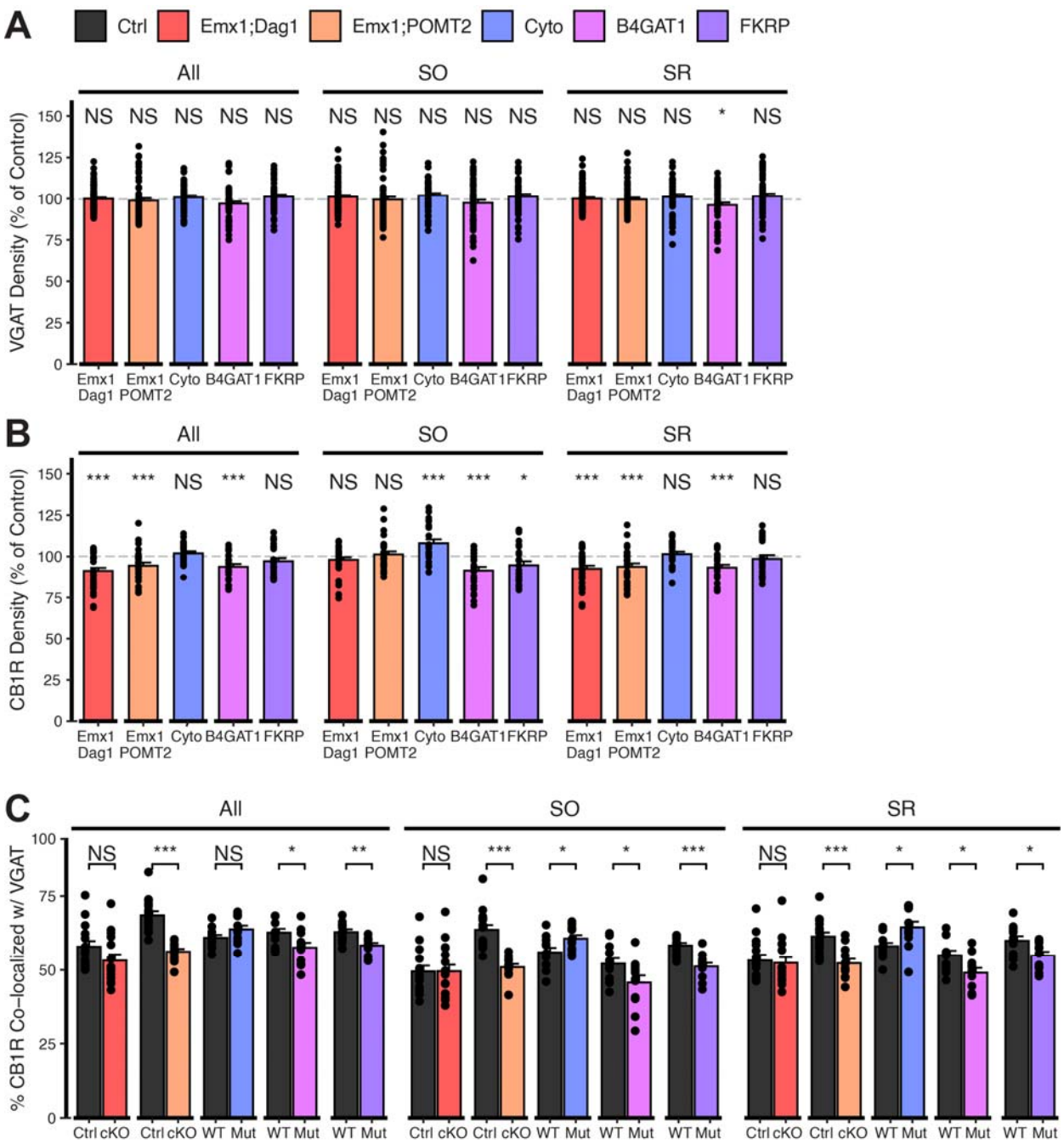

Supplementary Figure 5. Extended quantification of images in Figure 5A-C. Quantification within hippocampal CA1 SO and SR regions and all regions pooled together. **(A)** Quantification of VGAT puncta density expressed as a percent of control. **(B)** Quantification of CB_1R puncta density expressed as a percent of control. **(C)** Quantification of co-localization between VGAT and CB_1R to estimate putative CB_1R^+ basket cell synapse formation. Error bars show mean + SEM. (To see quantification of puncta densities and co-localization in SP see **Fig. 5D-F**.) See **Supplementary Table 1**

for Ns. *Significance: * = $p < 0.05$, ** = $p < 0.01$, *** = $p < 0.001$, NS = $p \geq 0.05$.*
Abbreviations: SO, stratum oriens; SP, stratum pyramidale; SR, stratum radiatum.

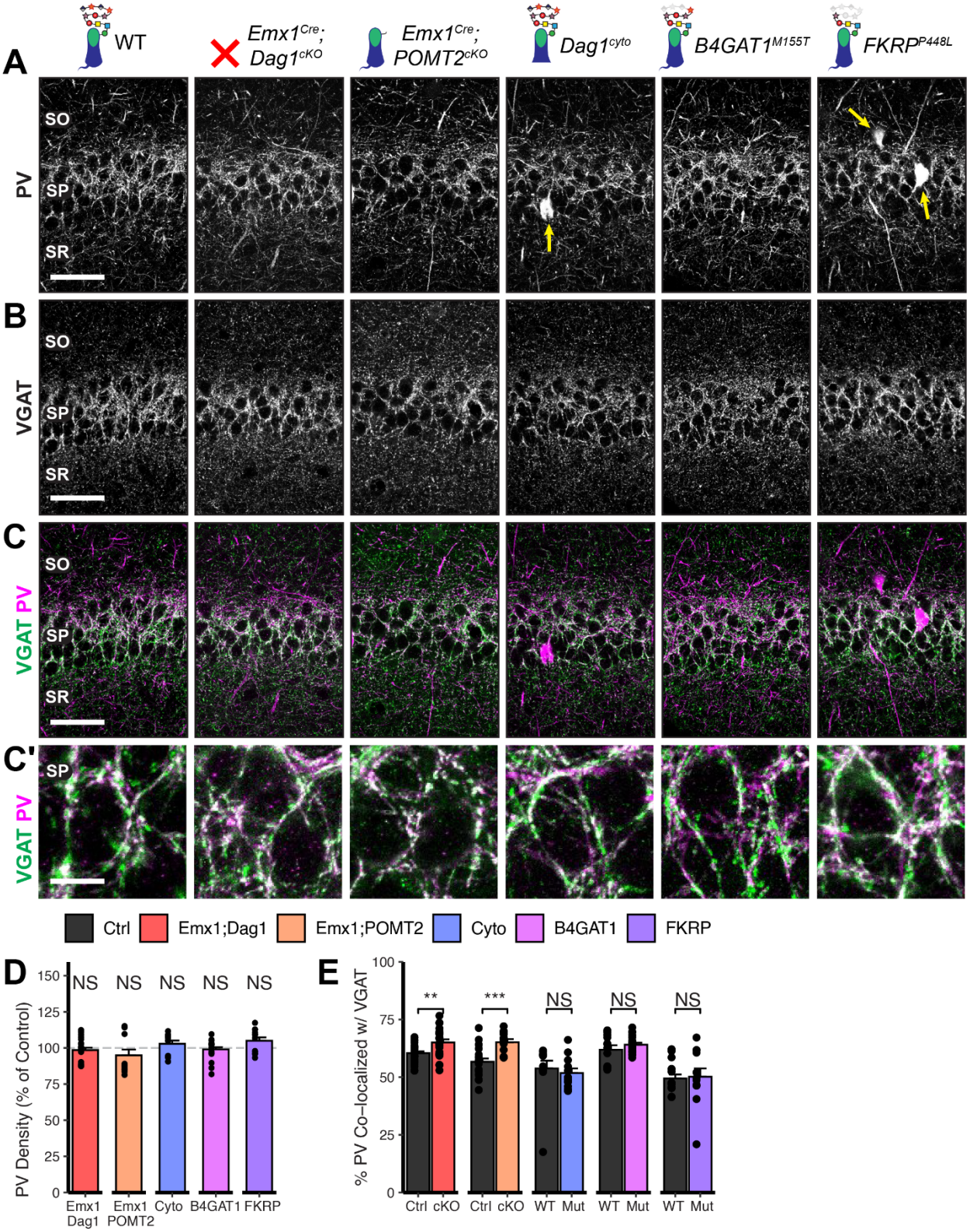

Supplementary Figure 6. *Dag1* and *POMT2* cKOs exhibit increased PV$^+$ basket synapse formation in *stratum pyramidale* of hippocampal CA1. P30 coronal sections immunostained for **(A)** PV and **(B)** VGAT in hippocampal CA1; merged image

in **(C)** shows PV in magenta and VGAT in green. Yellow arrows indicate PV^+ interneuron cell bodies. (A-C) Scale bar = 50µm. (Higher magnification view of SP in **(C')**; scale bar = 10µm.) **(D)** Quantification of PV puncta density in SP expressed as a percent of control. **(E)** Quantification of co-localization between VGAT and PV in SP to estimate putative PV^+ basket synapse formation. Error bars show mean + SEM. (To see quantification of puncta densities and co-localization in SO and SR see **Supplementary Fig. 6**.) See **Supplementary Table 1** for Ns. *Significance: * = $p < 0.05$, ** = $p < 0.01$, *** = $p < 0.001$, NS = $p \geq 0.05$. Abbreviations: PV, parvalbumin; SO, stratum oriens; SP, stratum pyramidale; SR, stratum radiatum.*

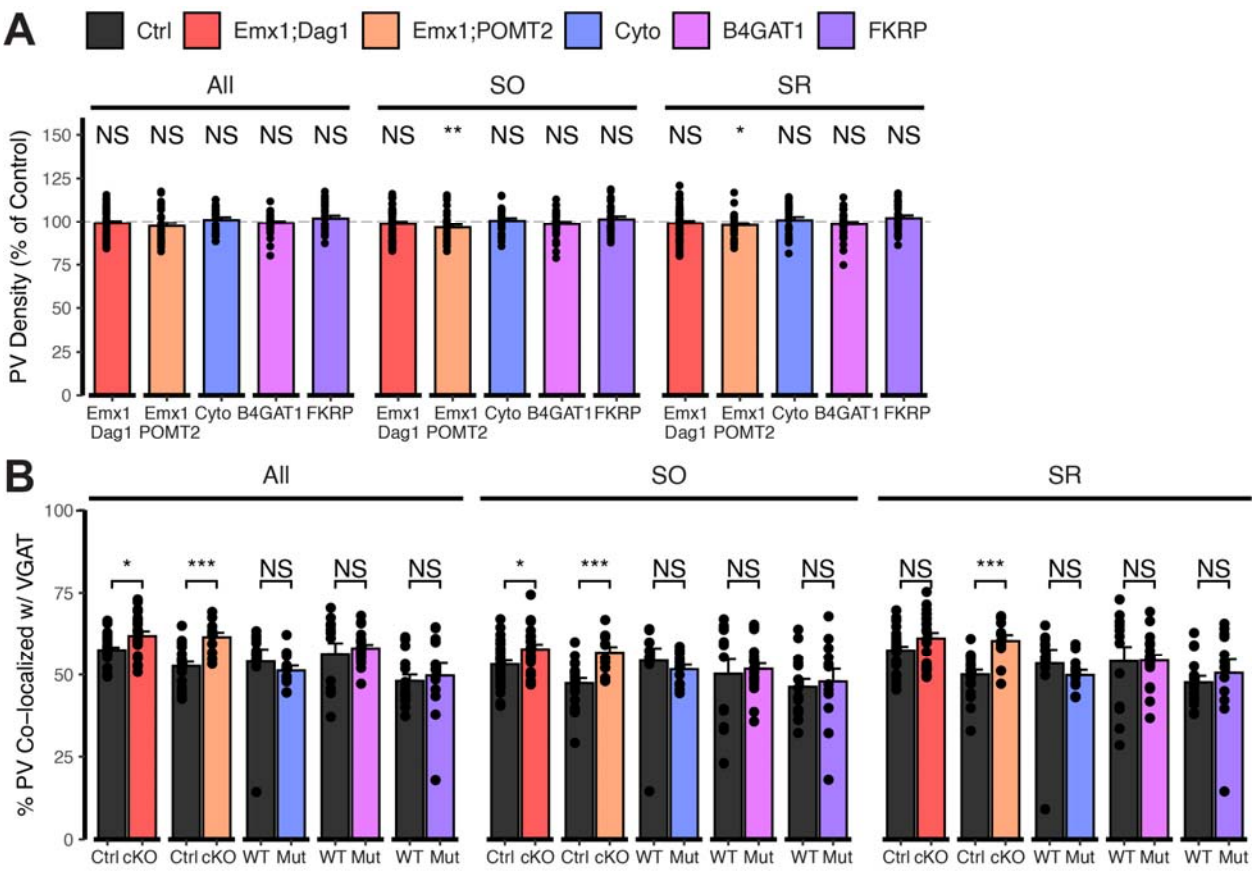

Supplementary Figure 7. Extended quantification of images in Supplementary Fig. 6A-C. Quantification within hippocampal CA1 SO and SR regions and all regions pooled together. **(A)** Quantification of PV puncta density expressed as a percent of control. **(B)** Quantification of co-localization between VGAT and PV to estimate putative PV^+ basket cell synapse formation. Error bars show mean + SEM. (To see quantification of puncta densities and co-localization in SP see **Supplementary Fig. 6D-E**.) See **Supplementary Table 1** for Ns. *Significance: * = p < 0.05, ** = p < 0.01, *** = p < 0.001, NS = p ≥ 0.05. Abbreviations: PV, parvalbumin; SO, stratum oriens; SP, stratum pyramidale; SR, stratum radiatum.*

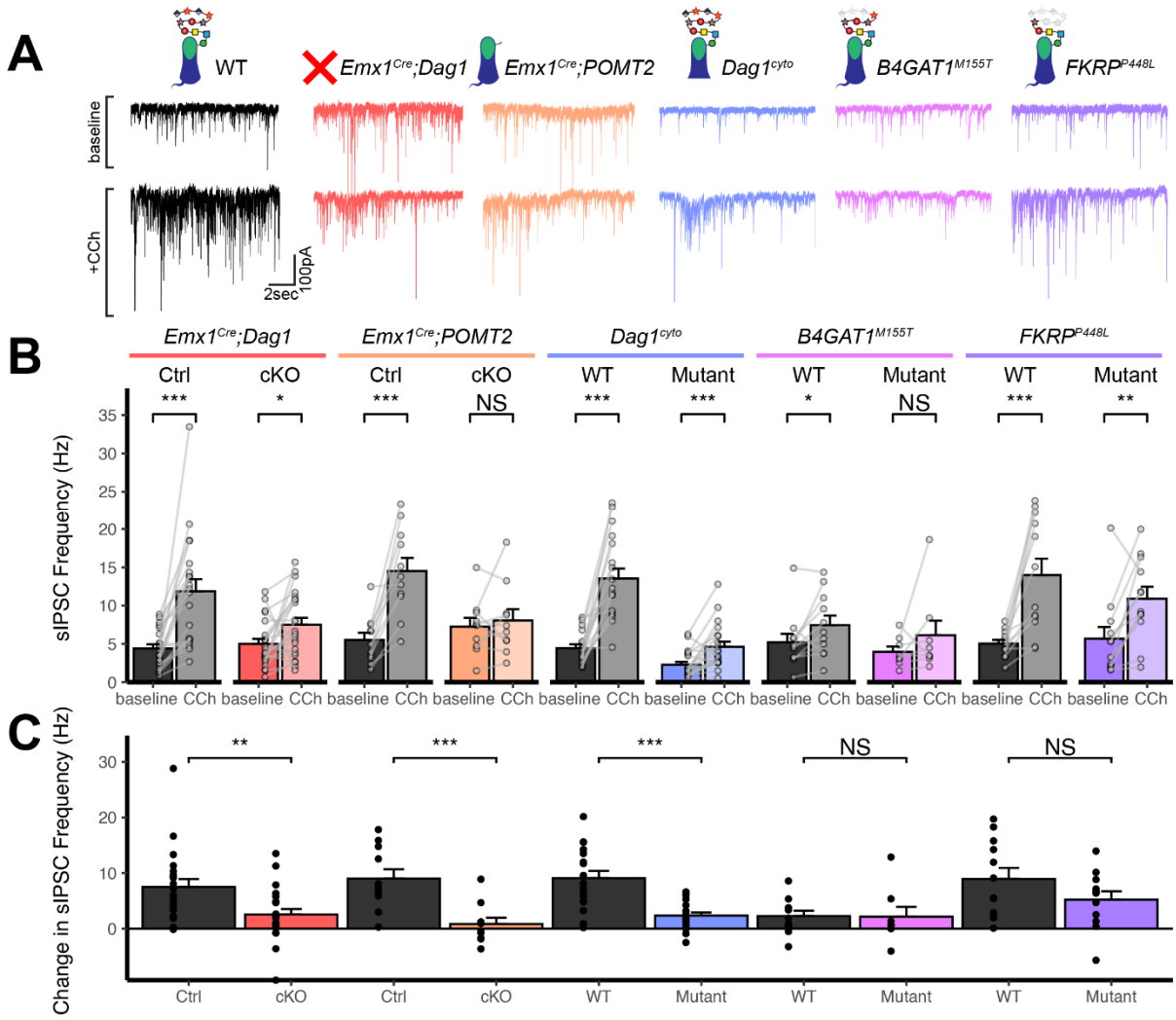

Figure 6. *Dag1* is required for CCK$^+$/CB$_1$R$^+$ IN synapse function in hippocampal CA1 in a manner dependent on both glycosylation and intracellular interactions. **(A)** Representative traces showing 15 seconds of sIPSC recordings at baseline (top) and after the addition of carbachol (bottom). **(B)** Quantification of average sIPSC frequency at baseline and after the addition of carbachol. **(C)** Quantification of the change in sIPSC frequency with the addition of carbachol. Error bars show mean + SEM. See **Supplementary Table 1** for Ns. *Significance: * = $p < 0.05$, ** = $p < 0.01$, *** = $p < 0.001$, NS = $p \geq 0.05$. Abbreviations: sIPSC, spontaneous inhibitory postsynaptic current; CCh, carbachol.*

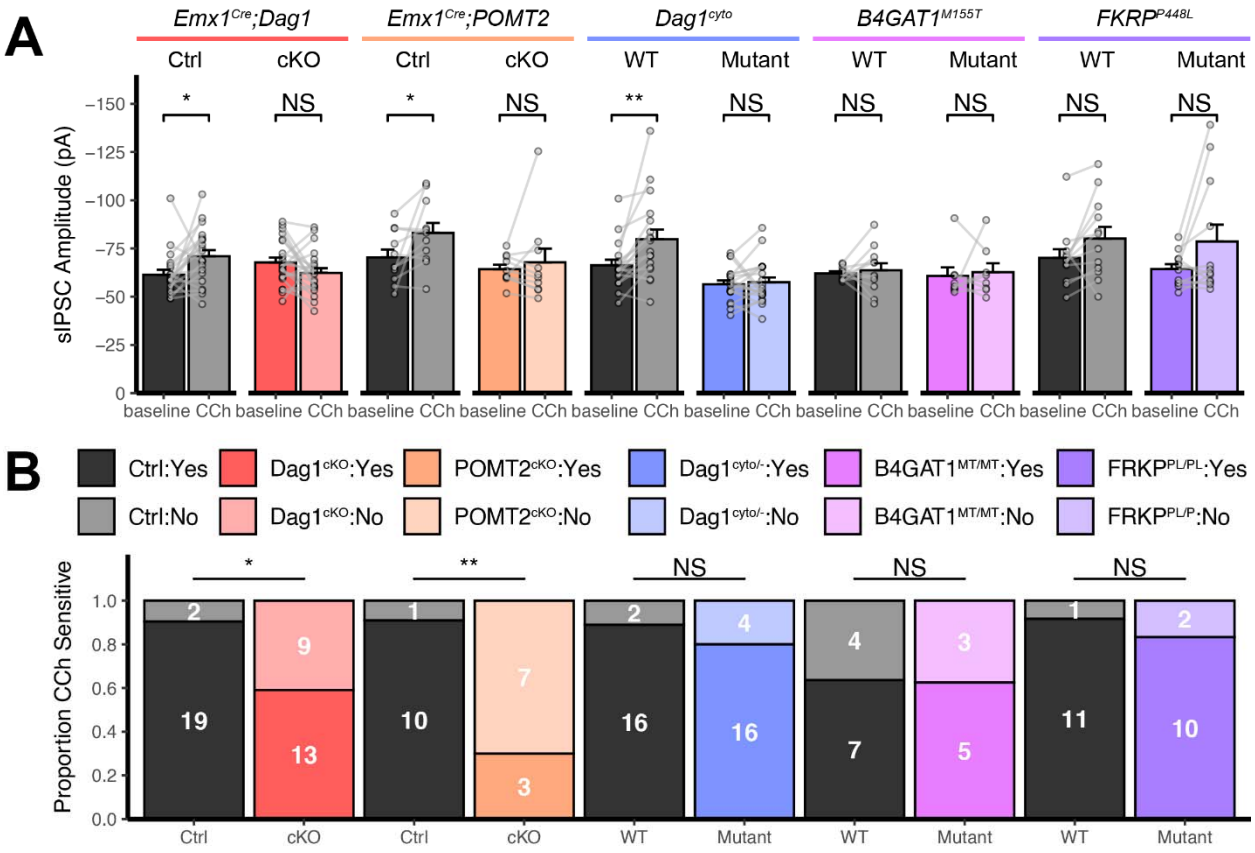

Supplementary Figure 8. Additional quantification of sIPSC recordings. (A) Quantification of average sIPSC amplitude at baseline and after the addition of carbachol. Error bars show mean + SEM. **(B)** Quantification of the proportion of carbachol-sensitive cells within each genotype. Non-responsive cells are shown in lighter color, responsive cells are shown in darker color. See **Supplementary Table 1** for Ns. *Significance: * = p < 0.05, ** = p < 0.01, *** = p < 0.001, NS = p ≥ 0.05. Abbreviations: sIPSC, spontaneous inhibitory postsynaptic current; CCh, carbachol.*

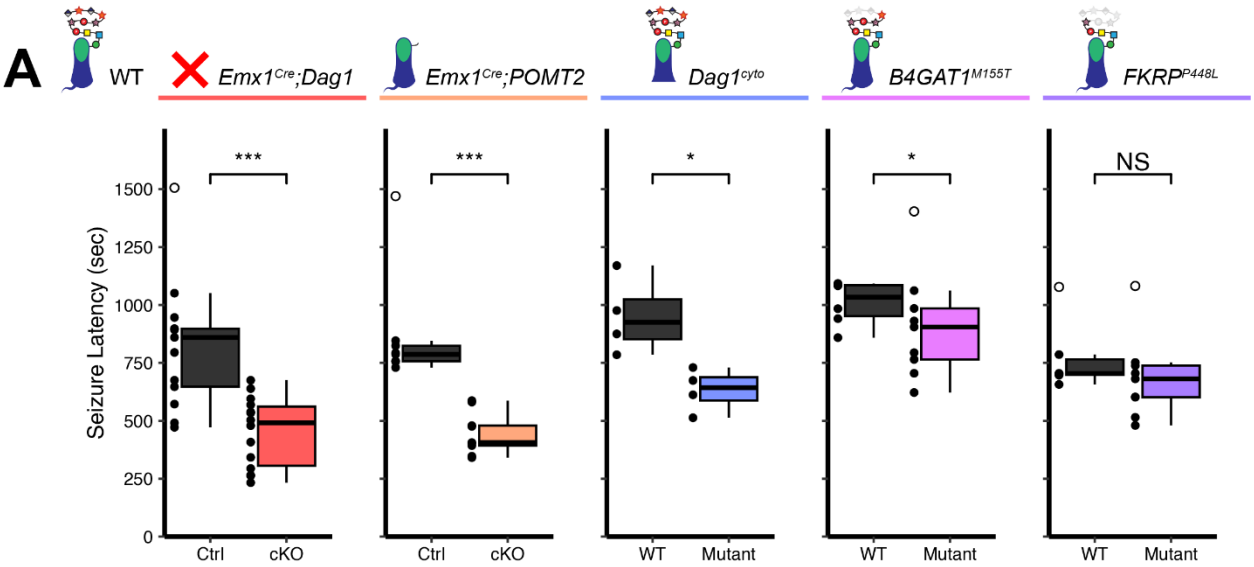

Figure 7. Reduced seizure induction threshold in models of dystroglycanopathy. (A) Quantification of latency (in seconds) to generalized tonic clonic seizure upon exposure to 10% flurothyl delivered at a constant rate. Open points denote statistical outliers. See **Supplementary Table 1** for Ns. *Significance: * = p < 0.05, ** = p < 0.01, *** = p < 0.001, NS = p ≥ 0.05.*

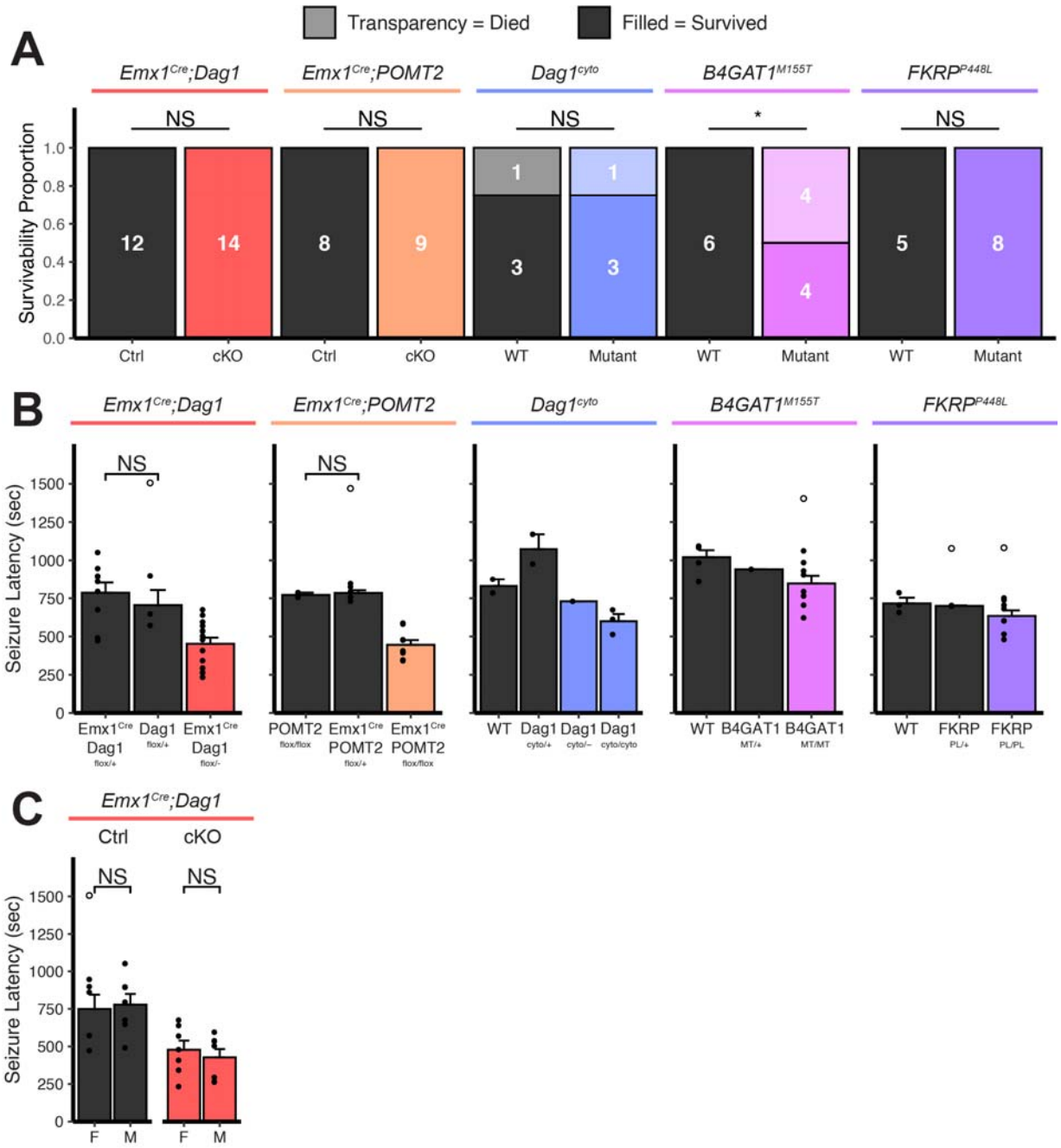

Supplementary Figure 9. Extended seizure induction threshold data.
(A) Proportion of mice that died as a direct result of a flurothyl-induced seizure. Survivors are depicted in darker colors, fatalities in lighter colors. **(B)** To minimize the number of animals needed for this experiment, certain genotypes were pooled together. Here we show that pooled genotypes are not different. Statistical tests were run where Ns were sufficient to provide meaningful comparison. **(C)** Seizure latencies split by sex. Note: only the *Emx1^{Cre};Dag1* group is powered sufficiently to statistically compare sexes. Open points denote statistical outliers. Error bars show mean + SEM.